RecV recombinase system for spatiotemporally controlled light-inducible genomic modifications

Ali Cetin*[†1], Shenqin Yao[†1], Ben Ouellette[1], Pooja Balaram[1], Thomas Zhou[1], Marty Mortrud[1], Soumya Chatterjee[1], Yun Wang[1], Tanya L. Daigle[1], Bosiljka Tasic[1], Xiuli Kuang[2], Hui Gong[3], Qingming Luo[3], Shaoqun Zeng[3], Anat Kahan[4], Viviana Gradinaru[4], Hongkui Zeng[1]
[1]Allen Institute for Brain Science, Seattle, Washington, USA.

[2]School of Optometry and Ophthalmology, Wenzhou Medical College, Wenzhou, Zhejiang, China.

[3]Britton Chance Center for Biomedical Photonics, Wuhan National Lab for Optoelectronics, Huazhong University of Science and Technology, Wuhan, Hubei, China.

[4]Division of Biology and Biological Engineering, California Institute of Technology, Pasadena, California, USA.

[†]These authors contributed equally to this work.

*Correspondence should be addressed to A.C. (alic@alleninstitute.org).

Keywords:

Light-inducible, recombinase, recombination, RecV, Vivid, Cre, Dre, Flp

ABSTRACT

Brain circuits are composed of vast numbers of intricately interconnected neurons with diverse molecular, anatomical and physiological properties. To allow highly specific targeting of individual neurons for structural and functional studies, we modified three site-specific DNA recombinases, Cre, Dre and Flp, by combining them with a fungal light-inducible protein, Vivid, so that their recombinase activities can be driven by blue light. We generated viral vectors to express these light-inducible recombinases and demonstrated that they can induce genomic modifications in dense or sparse populations of neurons in live mouse brains controlled by one-photon or two-photon light induction. As an important application, we showed that light-inducible recombinases can produce highly targeted, sparse and strong labeling of individual neurons thereby enabling whole-brain morphological reconstruction to identify their axonal projection specificity. In addition to targeting cortical brain areas, we applied the method in deep targets, with a demonstration of functional calcium imaging. These molecular tools enable spatiotemporally-precise, targeted genomic modifications that will greatly facilitate detailed analysis of neural circuits and linking genetic identity, morphology, connectivity and function.

INTRODUCTION

To understand how a biological system works it is often useful to dissect it to its building blocks and define how those building blocks work together to generate its function. Mammalian brain is one of the most complex biological systems. It is composed of millions to billions of cells with diverse characteristics. To understand this extraordinary complexity, it will be essential to define cell types based on properties such as gene expression, morphology and physiology at single cell level. Furthermore, the unique properties of individual cells need to be related to their connectivity patterns and their activities in a behavioral context. Anatomical information combined with genetic identity and functional properties at the single cell level will enable better analysis of brain circuitry underlying complex behaviors in health and disease.

One of the most powerful approaches to characterizing cell types and studying their functions relies on mouse genetics[1]. Strategies that rely on transgenic or viral expression of recombinases allow a highly specific level of genetic modification[2-4]. Multitude of cell type-specific Cre recombinase mouse lines has led to many discoveries in neuroscience over the last few decades. Further improvements on spatiotemporal control can allow much higher resolution manipulations and studies of biological systems.

Currently finding individual cells/neurons *in vivo*; characterizing and genetically manipulating them for targeted genomic modifications as well as expressing genes in a targeted manner is challenging to execute in an efficient manner. The state of the art for introducing an exogenous gene to a specific neuron is to get close to the neuron of interest using glass capillaries and introduce the agent of interest either by the patch clamp technique[5] or via applying electric pulses[6,7]. However, these techniques are highly challenging and usually result in low and variable yields. Low levels of recombination can be achieved by lowering the dose of inducers (*e.g.*, tamoxifen, in the case of CreER) or 'inefficient' recombinase reporters (*e.g.*, MADM[8]). However, the sparse genetic modification achieved using these methods is random and cannot be easily directed to specific cells of interest.

Light is a particularly powerful and versatile regulator with its tremendous adjustability in the dimensions of spectrum, intensity, space (location and size) and time (timing and duration). Using photons to access and genetically modify individual neurons will offer an improvement over the current state-of-the-art. Multi-photon additive characteristics of light that can generate a spatiotemporally-restricted excitation is well suited to fine spatial control[9]. Thus, modifying current genomic manipulation enzymes to make them light inducible could be an ideal approach to reach a high spatiotemporal resolution for targeted single cell manipulations.

To date several light inducible protein-based spatiotemporal control systems were developed[10-32]. These systems depend on various light sensing modules to control cellular mechanisms with approaches ranging from targeting of protein states, localization, transcription and genetic alterations. To leave a permanent genetic mark in individual cells in this study, we developed and validated light inducible site specific recombinase systems and its associated set of viral tools via comparing and optimizing various light inducible systems with the criteria that they induce robust genomic modifications with no or minimally detectable background under no-light condition. Our work resulted in generation of highly efficient light inducible versions of the most commonly used site-specific recombinases -Cre, Dre and Flp - that allow tight *in vivo* opto-genomic modifications.

RESULTS

A Split Vivid-Cre enables efficient light-inducible site-specific DNA modification

To spatiotemporally regulate site-specific recombination, we generated a light-inducible genetic switch based on a fungal light sensitive protein – Vivid (VVD)[33]. To generate light inducible recombinases we chose the VVD protein (**Fig. 1a**) mainly because it is the smallest (450 bp) of all Light Oxygen or Voltage (LOV) domain-containing proteins, and therefore suitable for fitting into viral vectors with limited genomic capacity. In addition, the spectral properties of VVD, namely the fact that its excitation and emission drops sharply to near 0 with light above ~520 nm (**Fig. 1b**), would allow us to use other fluorescent proteins, activity indicators or optogenetic molecules that work at longer wavelengths[19,34].

Upon blue light illumination, VVD forms a homodimer[34] due to conformational changes induced by Flavin Adenine Dinucleotide (FAD) cofactor within the LOV domain. The FAD cofactor within the LOV domain has a peak single-photon (1P) excitation at 450 nm and peak two-photon (2P) activation at 900 nm wavelength[35]. LOV domain evolved in *Neurospora crassa* to allow the adaptation to increasing luminescence levels and regulation of circadian rhythms[36]. The crystal structures of both monomer and dimer forms of the protein have been solved[37] (**Fig. 1a**). The crucial step in the dimer transition is the photo-induced cysteinyl-flavin formation and initiation of a hydrogen bonding cascade which unleashes the N-terminus of the protein from the core, exposing the dimerizing binding pocket of the protein[37]. Conformational changes in the N-terminal Cap Per-ARNT-Sim (PAS) domain gate the structural alterations leading to the dimer formation[34]. Majority of the conformational changes take place within the N-terminal latch, the first alpha helix, and the beta chain of the protein.

To generate a precise spatiotemporal control of gene expression, we used a split-Cre recombinase system[19,38-40] and turned it into a light-inducible system using the VVD protein (**Fig. 1c**). We named these new proteins CreV, and the general light-inducible Vivid-recombinase system RecV.

For Cre recombinase to function properly the N terminus and the C terminus of the protein need to come in close proximity and form the correct tertiary structure. The crystal structure of Cre is known[41] and so are the crystal structures of both dimer and monomer versions of VVD[34,37]. In the dimer form, the N terminal portion of one VVD protein gets into close proximity to the C terminus of the other (**Fig. 1a**). Our design for CreV, guided by this information, attempted to bring together the N and C termini of Cre in the correct orientation only upon light-induced conformational change and dimerization of VVD. To split the Cre protein, we relied on previous reports of the GCN4-coiled coil domain-based split Cre system, since this system was shown to generate stable dimers[38]. To achieve light inducibility, we fused the inactive N-terminal 19-59 amino acid segment of Cre to the N terminus of one VVD monomer. In parallel, we combined the remaining inactive 60-343 amino acid segment of Cre to the C terminus of another VVD monomer, which we codon diversified to reduce the sequence similarity of the two constructs and minimize the risk of recombination when they are co-expressed. We also added penta-Glycine (5G) chains as linkers between the Cre portions and VVD monomers to maximize the flexibility and help two Cre domains assemble in the proper orientation.

To test these constructs, we cloned each into a recombinant adeno-associated virus (rAAV) expression vector driven under the human elongation factor 1 alpha (EF1a) promoter (long version)[42]. The resulting NCreV and CCreV constructs along with a dTomato-expressing Cre reporter construct, EF1a-Flex-dTomato (**Fig. 2a** and **Supplementary Fig. 1**) were co-transfected into HEK293T cells and robust light-inducible recombination could be observed with 458 nm blue light induction compared to the no-light condition (**Fig. 2b,c**). The VVD absorbance decreases sharply above 520 nm of wavelength[19] (**Fig. 1b**), thereby allowing us to conduct experiments in red light conditions.

Vivid-based light-inducible system created for the Dre recombinase

As a next step, we decided to broaden the capabilities of the RecV approach by modifying another site-specific DNA recombinase. This is especially important since it would allow us to utilize already existing Cre driver mouse lines to study Cre-defined populations and to develop intersectional strategies to further refine cell type-specific genetic manipulation. For this we turned to a relative of Cre recombinase, the Dre recombinase[43].

Dre recombinase from a P1-like phage recognizes a different site from Cre – called Rox[44]. However there still is a certain level of homology between the two enzymes. We reasoned that the sequences surrounding the homology region (**Fig. 1d**) within Dre N-terminus, where we split Cre into two non-functional compartments, could also be targeted to generate a split Dre. We specifically disconnected residues after the consensus SWAaWC at the very end of the N terminal portion of Cre – the transition of arginine to glutamine, like the split Cre system.

We custom synthesized the two Dre-VVD components and tested the newly formed DreV (NDreV + CDreV) for the dimerization-induced efficacy of recombination in HEK293T cells. To assess DreV activity, we also developed an inverted Rox sites flanked dTomato-expressing Dre reporter construct, EF1a-Frex-dTomato (**Fig. 2a** and **Supplementary Fig. 1**). Our results indicate that the light-induced DreV recombination is efficient in HEK293T cells in transient transfections, and is similar to CreV (**Fig. 2b,c**).

Spatiotemporal regulation of gene expression can be further fine-tuned using 2P excitation since it has a much narrower point spread function in the axial direction. We tested if the VVD based recombination can take place using 2P light under cell culture conditions. Our results indicate that DreV-mediated light-inducible recombination can indeed be achieved by application of 900-nm wavelength of 2P light at the center of cell culture plates as revealed by RFP fluorescent reporter expression (**Supplementary Fig. 2**).

Single expression construct designs for CreV and DreV

To implement the RecV strategy efficiently and reduce the number of viruses or transgenic mouse lines needed to be made, it is preferable to co-express the two halves of RecV in a single construct. To achieve this, we tested a variety of ways to link the N and C components of CreV or DreV that would provide the highest efficiency of recombination with the least amount of background recombination.

First, we generated a single open reading frame construct in which inactive N and C termini of Cre recombinase were fused to a single VVD protein such that when the dimerization occurs, the N and C termini of Cre should get close together (NCre-VVD-CCre). To increase flexibility to the N or C termini, we made variations of this design by addition of 5 glycine residues to either the N or C terminal portions combining the Cre components and VVD (NCre-5G-VVD-CCre and NCre-VVD-5G-CCre). However, high level of background recombination in the absence of light was observed in all 3 cases (**Fig. 3a,b**). This occurred likely because the N and C termini of the proteins were close enough that despite the insertion of VVD in between, they could interact and recombine the LoxP sites in the absence of light. We tried reducing the number of glycine residues in NCre-5G-VVD-CCre and NCre-VVD-5G-CCre to 4, 3, 2 and 1 but did not observe significant improvements (data not shown). We did not try adding 5G to both N and C terminal joints since we reasoned trying to increase flexibility could only worsen the background.

Next, we generated co-expression constructs relying on a ribosome skipping, cis-acting hydrolase element PQR (P2A variant 3) that was shown to efficiently generate independent proteins in a ratiometric protein quantification screen[45]. We added this sequence between the open reading frames of NCre-5G-VVD and VVD-5G-CCre with both orders (named NCreV-PQR-CCreV and CCreV-PQR-NCreV), and tested them with the same reporter assay. Background recombination levels with these constructs were minimal, however, the light induction levels were relatively low (**Fig. 3a,b**). There were 24 amino acids from the PQR sequence added to the end of the first protein in each case, and we reasoned these amino acids may have interfered with the protein activity.

Finally, we generated two bi-cistronic expression cassettes in which an internal ribosome entry sequence (IRES), which allows translation initiation from within the transcript, was inserted in between NCre-5G-VVD and VVD-5G-CCre with both orders (NCreV-IRES-CCreV and CCreV-IRES-NCreV). Among these constructs the highest level of expression upon light induction with minimal levels of background recombination was the CCreV-IRES-NCreV construct (**Fig. 3a,b**). While using the IRES co-expression strategy the second protein within the bi-cistronic unit may be translated in lesser amount, increased CCreV to NCreV ratio may allow higher efficiency of the light-induced recombination.

Since for CreV the best light-inducible construct with the least background was CCreV-IRES-NCreV, we decided to generate the DreV version of this configuration as well. This construct (CDreV-IRES-NDreV) gave similar level of induction with light as the equivalent CreV version (**Fig. 3a,b**).

Addition of a drug inducibility option to the RecV system

For many *in vivo* and *in vitro* experiments in addition to the light control, a ligand mediated induction step can enable further temporal regulations. For example, it can allow combinatorial studies in which imaging/stimulation methods (*e.g.*, using GCaMP6 or channelrhodopsin) using wavelengths overlapping with VVD are conducted sequentially with RecV-mediated recombination. It can also reduce spurious or unwanted light-induced recombination events (e.g. during early mammalian postnatal development, in transparent model organisms, etc.). To avoid unwanted recombination research can be conducted under red light conditions since it doesn't effectively activate VVD, in some cases it may not be desirable to use this approach because systems such as vision depend on normal light exposure to develop and function properly. For this reason, we utilized a blood brain barrier permeable small molecule ligand inducible system, the trimethoprim (TMP) inducible bacterial dihydrofolate reductase (DHFR) system in which free DHFR is degraded (destabilized) in cells whereas TMP-bound DHFR is stabilized.

A TMP-inducible DHFR-Cre system was previously reported[46]. Similarly, here we fused DHFR to the N terminus of the DreV recombinase to produce a destabilized DreV which can then be stabilized with administration of TMP. We combined this N-terminal half with the C-terminal half of the "normal" version of DreV to produce CDreV-IRES-DHFR-NDreV (**Supplementary Fig. 1**). We generated a Cre dependent construct for CDreV-IRES-

DHFR-NDreV so that it can be used (for example, to generate mouse lines) for combinatorial studies with already existing Cre driver lines. *In vitro* testing of this construct together with a Cre driver plasmid in transiently transfected HEK293T cells demonstrated that this recombinase can be regulated by both light and the small ligand TMP (**Fig. 3c**).

A new RecV variant with further improved light-induction efficiency

A variation of the VVD system was previously reported, in which mutations were introduced to create a heterodimer VVD system (the Magnet system)[12]. The benefit of the heterodimer system in theory is to minimize any detrimental effect caused by homodimers. In a follow-up study[32] the same VVD mutants were used to generate a light-inducible Cre recombinase. Though no comparison to wild-type VVD was made, notably optimizations with linkers as well as the nuclear localization signals (NLS) and P2A elements led to significant improvements in light induced recombination efficiencies. Thus we tested if the same strategy can also help to enhance the efficiency of our wild-type VVD-based RecV system.

To compare the Magnet system with wild-type VVD as well as to test the benefit of adding the NLS and the additional linkers, we generated PhotoActivatable(PA)-Cre[32] (PA-Cre-Magnets) and PA-Dre (PA-Dre-Magnets) expressing constructs that included the reported heterodimerizing Magnets, NLS, linkers as well as the P2A elements (**Supplementary Fig. 1**). We also generated wild-type VVD based versions of these same constructs by replacing the Magnet-VVD variants with wild-type VVD, which we named PA-improved(i)CreV and PA-iDreV (**Supplementary Fig. 1**). Note that to make the conditions as comparable as possible we used the P2A element instead of PQR in these new constructs. We tested these four constructs along with the split CreV and DreV constructs in HEK293T cells using fluorescent recombinase reporters (**Fig. 4**). Both PA-Cre-Magnets and PA-Dre-Magnets gave significant amount of background recombination in the absence of light, while with light they have more efficient inducibility than the split CreV and similar efficiency to the split DreV constructs. On the other hand, the wild-type VVD containing counterparts PA-iDreV and PA-iCreV exhibited control levels of recombination in the absence of light and retained high levels of inducibility – ~1.6 fold higher for PA-iCreV as compared to split CreV and ~0.6 fold lower for PA-iDreV as compared to split DreV in relative fluorescence intensities.

In our tests, we documented that CCreV-IRES-NCreV and CDreV-IRES-NDreV constructs gave very similar recombination rates (around 3-fold over baseline) compared to un-induced Magnets *in vitro*. When injected into brains (see below), CCreV-IRES-NCreV and CDreV-IRES-NDreV containing AAVs induced significant amount of recombination upon light induction. Because of this we reasoned that un-induced leaky Magnets are likely to drive significant amount of background recombination *in vivo*, thus we did not further pursue that approach.

In addition to comparing the Magnet-based light inducible Cre recombination system, we compared an improved cryptochrome, CRY2, based light inducible Cre recombination system[31], which is an alternative light inducible Cre recombination system, with PA-iCreV. Side by side comparison *in vitro* revealed that PA-iCreV performs ~4 fold better after 60 minutes of light stimulation than the CRY2 system, whereas CRY2 based Cre recombination system allows only a slight increase over baseline recombination (~1.2 fold) (**Supplementary Fig. 3**).

Our results indicate that wild-type VVD containing PA-iCreV and PA-iDreV constructs, which we call iCreV and iDreV for simplicity in the rest of our study, are better suited for co-expression of the multiple components of the RecV system as compared to the other co-expression constructs.

Generation of a light inducible Flp recombinase through a dimerizer screen

To increase intersectional genomic modification possibilities, we turned into a third widely used site specific DNA recombinase: Flp[47]. Previously there has not been a report describing a split Flp with non-functional halves that can become functional upon dimerization. There isn't enough sequence similarity between Flp, a recombinase from yeast, and Cre or Dre, recombinases from bacterial phages to guide a split based on homology. Thus, we resorted to structure-based *de novo* design of potential splitting sites for Flp. Crystal structure of the Holliday

junction bound Flp recombinase was resolved[48]. Using a more efficient codon optimized variant of Flp (FlpO)[49]; we made Flp splits at 21 loop locations that are transitions of alpha helices and beta sheets with hopes to not alter overall functionality within the dimer form (**Fig. 5a**). We generated VVD-fused split iFlpV constructs using the iCreV backbone by replacing the N and C termini of Cre with the 21 split Flp variants (**Supplementary Fig. 4**).

After gene synthesis, these constructs were cloned into CMV promoter driven mammalian expression plasmids and tested for light induced recombination in HEK293T cells via transient transfections along with a Flp dependent dTomato expressing reporter plasmid (**Supplementary Fig. 1**). Among the 21 variants, iFlpV2, 15, 19 and 20 gave the most significant light-induced recombination, with iFlpV2 giving a recombination of 11-fold increase in relative fluorescence intensity (**Fig. 5b**). The dark conditions of all these cases were almost identical to the controls indicating that, like iCreV and iDreV, the background recombination is almost non-existent (**Fig. 5b**).

In vivo light-inducible recombination of RecVs through local viral infections

To characterize this system within the mouse nervous system *in vivo*, we generated rAAVs from the plasmids carrying the N and C components of VVD-Cre (NCreV and CCreV) and VVD-Dre (NDreV and CDreV), as well as Cre or Dre reporters (**Supplementary Fig. 1**).

We co-injected the NCreV and CCreV rAAVs into the visual cortex of wild-type mice along with a Cre reporter rAAV (**Fig. 6a**) or into a Cre-reporter mouse line expressing EGFP, Ai139[50] (**Fig. 6b**). After two weeks of viral expression, the experimental mice received 30 min induction from a white halogen light source across the skull, exposed by cutting open the overlaying skin. Both experimental and control mice were left for further Cre-induced expression for an additional 2 weeks. Robust fluorescence was observed in the experimental mice in hundreds of neurons within the injection site. In contrast, we observed only a few fluorescent cells in controls.

Similarly, we co-injected the NDreV and CDreV rAAVs into the visual cortex of wild-type mice along with a Dre reporter rAAV (**Fig. 6c**) or into a Cre/Dre double reporter mouse line Ai66[51] along with a Cre-expressing rAAV (**Fig. 6d**), and observed robust light-induced recombination in both cases. When compared with CreV, DreV recombinase, at similar rAAV concentrations and within multiple sites and animals, could induce recombination in higher number of neurons (and in almost all neurons proximal to the injection site), similar to a pattern of recombination a native uninterrupted Cre or Dre virus can accomplish.

To test the light-induced recombination efficacy of the IRES based single RecV designs we generated rAAVs for both CCreV-IRES-NCreV and CDreV-IRES-NDreV. Both versions of these viruses resulted in noticeable amounts of recombination upon light induction within the injection sites in Ai14 (a Cre-dependent tdTomato-expressing mouse line[52]) and Ai66R mice (a tdTomato-expressing reporter mouse line that is solely dependent on Dre[50]) (**Fig. 6e,f**).

To precisely perform light inducible genetic manipulations for detailed study of the intact brain circuits and individual neurons, restriction of light to certain areas and cells using 2P light is advantageous. We tested *in vivo* 2P light inducibility through a light accessible cranial window. A mixture of four viruses – a Dre-dependent dTomato-expressing rAAV, a control EGFP-expressing rAAV, and the NDreV and CDreV rAAVs – were injected into primary visual cortex of a wild-type mouse. Two weeks after 2P light induction, recombination could be observed within the layer (2/3) where 2P light stimulation was applied, whereas co-injected control EGFP-expressing virus labeled multiple layers (**Fig. 6g**). Notably in none of our regular viral expression experiments we saw such a clear planar expression of fluorescent reporters restricted to Layer 2/3 (**Fig. 6a-f**). Thus, these results suggest that 2P-mediated light-inducible RecV recombination can be highly precise, potentially will allow targeted single cell recombination in the future.

Whole brain infection and localized light induced recombination with RecVs

Recently a new blood brain barrier permeable rAAV serotype, PHP.eB, was reported to be effectively infecting large proportions of the entire nervous system in mice after retroorbital delivery[53]. Since this technique allows systemic administration for widespread transgene expression in the entire brain, we reasoned it could be an excellent rapid testbed for examining RecV constructs in the entire mouse brain to see if there is any background recombination in the absence of light in any part of the brain as well as to test local light inducibility of recombination.

For this purpose, we generated a regular EF1a promoter-driven Cre-expressing rAAV as well as RecV rAAVs using PHP.eB serotype. We found that PHP.eB EF1a-Cre virus, when injected intracerebroventricularly (ICV) instead of retroorbitally into the Ai14 mice, can still infect the entire brain (**Fig. 7a**). To our knowledge this is the first demonstration of effective PHP.eB mediated gene delivery into the nervous system using the ICV route. This method may help save virus, further restrict the infection to nervous system and may overcome obstacles related to intravenous delivery of genes for both basic research as well as gene therapy field applications in the future.

Following injection of the NDreV and CDreV virus mixture into the right ventricle of the Dre-dependent Ai66R mice, 2 weeks after light stimulation was made to the left hemisphere a gradient of recombination could be observed from the top of the left hemisphere to deeper layers (**Fig. 7b**). Deeper brain structures and sites far from the light stimulation did not have any fluorescently labeled cells, indicating that the technique allows highly specific light-inducible recombination with no background recombination. In addition, we tested the more efficient iCreV driven by the EF1a promoter with PHP.eB serotype in a Cre-dependent nuclear tdTomato expressing reporter mouse line Ai75. Very similarly we observed substantial recombination in the hemisphere of light stimulation contralateral to the ICV injection site (**Fig. 7c**). We also tested iDreV in the same way and obtained similar results (**Fig. 7d**).

We also tested *in vivo* efficiency of the iFlpV recombinase. In a tdTomato-expressing Flp reporter mouse line, AI65F. Following ICV injection of the PHP.eB serotyped iFlpV rAAV we could observe robust recombination in the light stimulated hemisphere (**Fig. 7e**). Similar to iCreV and iDreV there was no observable spurious background recombination at sites far from light stimulation.

One of the major advantages of generating multiple recombinases with independent recombination activity is that one can utilize them for intersectional targeting of cell types. For example, this can be achieved by using already existing Cre lines along with Cre/Flp dependent reporter viral vectors or mouse lines. To test the feasibility of this approach we injected PHP.eB iFlpV viruses into layer 5 pyramidal neuron specific Rbp4-Cre mice together with a Cre/Flp dependent reporter viral vector. After unilateral light stimulation we could observe layer 5 pyramidal neuron specific reporter gene expression in these mice (**Fig. 7f**).

Finally, we tested feasibility of light inducible recombination within a deeper brain area, striatum. Deep imaging or recording is more challenging due to tissue damage and blood clotting; both create obstacles to the light to pass through the tissue. By utilizing 1P light through an optical fiber we were also able to induce local recombination via iCreV in the striatum of Ai162 GCaMP6s Cre reporter mice[38], and record changes in fluorescence due to calcium concentration dynamics before and after light stimulation (**Fig. 8a-d**). Due to the localized illumination, GCaMP6s is expressed directly under the fiber, in comparison to the wide expression of tdTomato which was expressed constitutively under the CAG promoter (**Fig. 8b**). This expression pattern is a benefit for calcium imaging and recording, as it allows expression directly at the desired location. In addition, we utilized GRIN lenses[54] and induced recombination via local stimulation using 2P light together with local, non Cre dependent, expression of ChR2-eYFP, in C57Bl/6N mouse. Results indicate that a robust and local recombination can be achieved at the site of illumination (mCherry, **Fig. 8g**), side by side with ChR2 expression (eYFP). The highest expression of the Cre-dependent virus (mCherry) is ~ 750 µm below the lens tip (**Fig. 8f**), and we anticipate that this property depends on the type of GRIN lens. Our results show that light mediated genomic modifications can be efficiently spatiotemporally regulated *in vivo* in deep targets, providing a tool for an accurate expression of GCaMP6s under the optical device, as well as the possibilities for opsin expression.

RecV-mediated sparse labeling enables whole-brain reconstruction of single neuron morphologies

The development and *in vivo* validation of the light-inducible recombinase system (RecV) opens doors to many applications. Here we present several of such applications, mainly using light to control the precise location and number of neurons labeled to achieve the desired sparsity of targeted neuronal populations for the visualization, functional imaging as well as reconstruction of single neuron morphologies across the entire brain to understand their axonal projection specificity.

As shown above, CreV mediated *in vivo* reporter expression using a Cre reporter mouse line Ai139 resulted in strong expression of GFP in multiple cortical layers (**Fig. 6b**). Ai139 is a TIGRE2.0 reporter line expressing very high level of GFP (via tTA-mediated transcriptional amplification) allowing visualization of detailed cellular morphologies[50]. We tested if less light applied to the tissue could potentially induce sparse activation of the reporter gene expression while still retaining the high expression level. Such sparse but strong neuronal labeling would enable a very important application – whole-brain reconstruction of single neuron morphologies.

For this purpose, we injected the cortex of Ai139 mice with the 1:1 mixture of NCreV and CCreV rAAVs in serial dilutions and applied various durations of light across the skull to induce recombination in a sparse population of cortical neurons. We then imaged the whole brains using the fluorescence micro-optical sectioning tomography (fMOST) technique[55]. Lower dose of CreV viruses and shorter duration of light induction led to sparse and strong labeling of individual neurons (**Supplementary Fig. 5**). Sparseness was low enough that axons from many neurons could be traced. In the example brain shown in **Figure 9** (also see **Supplementary Movies 1 and 2**), 8 primary somatosensory cortical neurons were manually reconstructed. These neurons include 3 layer 2/3 pyramidal cells (PCs) with ipsilateral cortico-cortical projections, 2 layer 2/3 PCs with contralateral cortico-cortical projections, and 3 layer 5 thick tufted PCs with ipsilateral cortico-subcortical projections, revealing distinct axonal projection patterns.

In many cases where genetic access is not possible to restrict expression with conventional methods it is desirable to be able to further confine the region of recombination by precisely inducing it through localized illumination. To demonstrate this ability we performed headpost craniotomy and 2P assisted local laser stimulation experiments in trained head-fixed Ai139 reporter mice. To achieve sparseness, we used a 1:5 mixture of rAAV iCreV and rAAV tdTomato expressing viruses within primary visual cortex. In these experiments the virus that expresses tdTomato was co-injected both to guide our stimulation as well as to serve as a control of overall infection span. Our results indicate that local precise and sparse labeling of neurons is achievable using this method. Furthermore, due to the strength of the expression individual axons and boutons can be readily visualized without any need of immunohistochemical enhancement at sites very far away from where neuronal cell bodies are located, suggesting that whole neuron reconstructions can be achieved (**Supplementary Fig. 6)**.

DISCUSSION

Several versions of light-inducible Cre were reported previously[31,32,56], and they were mainly based on two types of light-inducible protein dimerization systems: CRY2-CIB1 and VVD. Initially reported CRY2-CIB1 system showed some promising *in vivo* results yet lacked high efficiency[56]. Since with this system light-induced recombination efficiency is relatively low and the sizes of the proteins are relatively large[17,21,32,57] we did not adopt it in this study. Recently, further optimization including the development of a long-lived photocycle mutant of CRY2-CIB1 improved dynamic range and efficiency of this system[31]. A direct comparison of this improved version and the VVD-based CreV system presented in this study shows that the CreV system is ~4 fold more efficient in fluorescence reporter assays. On the other hand, our results indicate that Magnet based light inducible Cre recombination is efficient, but it is also relatively leaky compared to VVD based counterpart. By incorporating the improved designs reported in the Magnet system[32] we were able to produce significantly more efficient RecV variants, iCreV, iDreV and iFlpV.

In our study, we chose to use the wild-type VVD and successfully applied it to not only Cre but also two other site-specific recombinases - Dre, through sequence homology analysis, and Flp, through structure-based analysis and screening of multiple split combinations, thus expanding the repertoire of genetic manipulation tools even further. We also showed that these light-inducible recombinases work highly efficiently and intersectionally in the brain to induce genomic modifications with no detectable background under conditions tested, and the location and number of cells modified can be regulated by varying light delivery conditions. Thus, we provide

proof of principle that RecV mediated light-inducible site-specific DNA modification works well in the mammalian nervous system. The viral tools we have already generated can be immediately useful for several applications.

The spatiotemporally selective targeting of cell populations or individual cells using light could allow fine-scale combinatorial functional, anatomical and circuit-level studies of cell type-specific networks. In addition to combining opsin expression with iCreV, and achieving efficient GCaMP6s expression using iCreV, the RecV viral vectors and Cre/Flp dependent iDreV or iFlpV mouse lines can be combined with existing cell type-specific genetic tools, and RecVs can also be used to generate new driver lines. With this approach one can envision performing a variety of combinatorial experiments including single cell activity imaging using genetically encoded voltage[58,59] or calcium indicators[60]; single cell monosynaptic rabies tracing[5,6] or targeted optogenetic and chemogenetic protein expression[61], all in a noninvasive or minimally invasive manner. The spectral and temporal separation as well as drug inducible versions could enable sequential investigations of functionally relevant cell populations, such as functional imaging using red calcium indicators first, followed by blue light mediated DNA recombination to selectively activate effector gene expression in specific cells of interest to examine their structure and connectivity and/or to perturb their function.

Another major improvement this methodology can bring is that one could perform loss/gain of function studies by switching genes off or on with much refined regional and cell type specificity and observing the lasting effects on physiology or animal behavior. One could also study development via switching genes with unprecedented temporal precision during the rapid cascade of events throughout the proliferation and differentiation processes. The half-life of the VVD homodimer is ~2 hours after brief light activation[12]. One could try to apply targeted light at very precise time points using standard or gentler *in utero* techniques. This is advantageous over the current CreER-based genetic fate mapping studies[62] in that it eliminates the side effects caused by tamoxifen and light-induced recombination is spatially and temporally much more precise. Furthermore, this approach could allow highly targeted network reconstructions by selectively labeling neurons in particular locations or having particular activity patterns or functional properties (*e.g.*, using 2P induction). Sparse expression of reporter genes using diluted Cre viruses or low doses of tamoxifen in CreER mice already exist. However, with RecV one could perform even more spatiotemporally restricted induction, and it can be combined with prior functional characterization using 2P imaging combined with drug inducible RecVs or red shifted calcium indicators in an intersectional manner.

The RecV approach can also be used in other species of interest in which light could be used to access individual cells of interest. For model systems in which germline genetic modification is feasible, the experiments can be designed to integrate multiple components of the described systems into the germline[51]. In model systems in which germline modification is not available, these experiments can be performed by using viral vectors in which a certain level of cell type specificity may be achieved by using short cell type specific promoters or enhancers[63,64], or target-defined specificity may be achieved with highly efficient retrogradely infecting designer viruses[65]. It is important to note here that not every genomic locus may be as accessible as the ones we tested. Thus, in the future it will be useful to do such tests in other loci and other model systems.

Overall, the broad range of potential applications show that the light-inducible recombinase system should enable much improved spatiotemporal precision and multiple combinatorial strategies in the micro- and macro-level analysis of neural circuits as well as in many other biological systems.

METHODS

Plasmid and virus construction for split RecVs

Sequences of NCre-5G-VVD, VVD-5G-CCre, NCre-5G-VVD-IRES-VVD-5G-CCre, VVD-5G-CCre-IRES-NCre-5G-VVD, NCre-5G-VVD-PQR-VVD-5G-CCre, VVD-5G-CCre-PQR-NCre-5G-VVD, VVD-5G-CDre-IRES-NDre-5G-VVD, NCre-Magnets-NLS-P2A-NLS-Magnets-CCre, NCre-VVD-NLS-P2A-NLS-VVD-CCre, NDre-Magnets-NLS-P2A-NLS-Magnets-CDre, NDre-VVD-NLS-P2A-NLS-VVD-CDre, and all iFlpV versions were chemically synthesized (GenScript, Piscataway, NJ). To screen poly-cistronic cassettes with the best light-inducible recombinase activity, N and C parts of RecV, as well as IRES-mediated, PQR-mediated and P2A-mediated RecV poly-cistronic cassettes were cloned into pCDNA3.1 with the CMV promoter (**Supplementary Fig. 1**).

To generate recombinant AAV viruses expressing split VVD-Cre (CreV) or VVD-Dre (DreV), the N or C part of CreV and DreV were cloned after the human EF1a promoter, followed by WPRE and hGH-polyA signal (**Fig. 2a** and **Supplementary Fig. 1**). To generate tandem co-expression RecV cassettes within the limit of AAV packing capacity, IRES-mediated poly-cistronic cassettes were cloned after the human EF1a promoter, followed by WPRE and duplicated short synthetic polyA (2xsPolyA) (**Supplementary Fig. 1**). The Cre reporters, pAAV-EF1a-Flex-dTomato or EGFP-WPRE-hGHpA, used pairs of double inverted LoxP and Lox2272 sites to flank the reporter dTomato or EGFP sequence. The Dre reporter, pAAV-EF1a-Frex-dTomato-WPRE-hGHpA, was generated by inserting an inverted dTomato sequence flanked with Rox sites after the human EF1a promoter, followed by WPRE and hGH-polyA signal (**Supplementary Fig. 1**).

21 iFlpV variants were generated with custom gene synthesis as follows: iFlpV1: 11 amino acids (aa) N and 412 aa C; iFlpV2: 27 aa N and 396 aa C; iFlpV3: 49 aa N and 374 aa C; iFlpV4: 67 aa N and 356 aa C; iFlpV5 72 aa N and 351 aa C; iFlpV6: 85 aa N and 338 aa C; iFlpV7: 95 aa N and 328 aa C; iFlpV8: 114 aa N and 309 aa C; iFlpV9: 129 aa N and 294 aa C; iFlpV10: 151 aa N and 272 aa C; iFlpV11: 169 aa N and 254 aa C; iFlpV12: 197 aa N and 226 aa C; iFlpV13: 208 aa N and 215 aa C; iFlpV14: 237 aa N and 186 aa C; iFlpV15: 251 aa N and 172 aa C; iFlpV16: 290 aa N and 133 aa C; iFlpV17: 318 aa N and 105 aa C; iFlpV18: 343 aa N and 80 aa C; iFlpV19: 374 aa N and 49 aa C; iFlpV20: 388 aa N and 35 aa C; iFlpV21: 408 aa N and 15 aa C. These constructs were cloned in pcDNA3.1 mammalian expression plasmids.

AAV1, AAV DJ and AAV PHP.eB serotype viruses were produced in house with titers of AAV1-EF1a-NCreV, 1.05 x 10^{12} genome copies (GC); AAV1-EF1a-CCreV, 5.16 x 10^{12}; AAV1-EF1a-NDreV, 4.20 x 10^{13}; AAV1-EF1a-CDreV, 5.40 x 10^{13}; AAV-DJ-EF1a-Cre, 2.00 x 10^{13}; AAV1-CAG-Flex-EGFP, 1.34 x 10^{13}; AAV-DJ-EF1a-Frex-dTomato, 1.90 x 10^{12}; AAV-DJ-EF1a-CCre-IRES-NCreV-WPRE-2xsPolyA, 7.7 x 10^{11}; AAV-DJ-EF1a-CDre-IRES-NDreV-WPRE-2xsPolyA, 1.6 x 10^{13}; AAV-PHP.eB-EF1a-Cre, 5.8 x10^{13}; AAV-PHP.eB-Syn-NDreV, 4.2 x 10^{13}; AAV-PHP.eB-EF1a-CDreV, 3.9 x 10^{13}; PHP.eB iCreV, 2.6 x 10^{13}; PHP.eB iDreV, 3.3 x 10^{13} and PHP.eB iFlpV, 2.7 x 10^{13} per ml.

Light activation in cultured cells

HEK293T cells were seeded into 6-well plates one day before transfection and reached 80% confluency on the day of transfection. Cells were co-transfected with a reporter expressing dTomato –for Cre and Flp- or dTomato- for Dre- for Cre, Dre or Flp mediated recombination and various constructs of split RecVs. Cells in the control groups were transfected with reporters alone. Each condition contained 4 replicates. Plates were kept in dark immediately after transfection. Twenty-four hours later, cells were exposed to blue light, and were then kept in dark immediately after light exposure. Cells were imaged for fluorescent reporter expression 48 hours after light induction, using an inverted fluorescence microscope. RecV activated dTomato expression in each condition was quantified using Image J.

TMP-mediated stabilization of DHFR-DreV

HEK293T cells were seeded into 6-well plates one day before transfection and reached 80% confluency on the day of transfection. To verify Cre-dependent expression of DreV and DHFR-DreV, cells were transfected with the Dre-dependent dTomato reporter and the Cre-dependent DreV expression cassettes, with or without the co-transfection of CMV-driven Cre. To test the efficiency of TMP-mediated stabilization of DHFR-DreV, RCL-DHFR-DreV-transfected cells were undergone medium exchange 6 h after transfection, either to fresh medium containing 10 μM of TMP or that containing the same volume of the solvent. Each condition contained 4 replicates. Plates were kept in dark immediately after transfection. Medium change was conducted with light off. Twenty-four hours later, cells were exposed to blue light, and were then kept in dark immediately after light exposure. Cells were imaged for dTomato expression 24 hours after light induction, using an inverted fluorescence microscope. CreV and DreV activated dTomato expression in each condition was quantified using Image J.

***In vitro* two-photon stimulation of DreV**

HEK293T cells were seeded into 35mm-plates one day before transfection. Cells were co-transfected with EF1a-eGFP, EF1a-Frex-dTomato, EF1a-NDreV, and EF1a-CDreV, with a ratio of 1:100:50:50. Two-photon activation was conducted at 48 hr after transfection at various conditions, and reporter expression was observed 36 hr post

stimulation. Two-photon activation conditions were as follows: λ = 900 nm, 90 mW, 1 ms/line (512 lines), 200 µm x 200 µm scan area, and duration of 3 to 15 mins. In one condition, randomly selected single cells were scanned in 5 areas, 36x36 µm each, separated by 40 µm roughly in a straight line across the plate with a duration of 1-10 seconds per area.

Surface/Cortical *In vivo* light activation

Stereotaxic injections were made into adult C57BL/6J (stock no. 00064, The Jackson Laboratory, Bar Harbour, ME) or transgenic reporter mice with a 1:1:1 or 1:1 mixture of three or two different rAAVs. For all experiments, animals were anesthetized with isoflurane (5% induction, 1.5% maintenance) and placed on a stereotaxic frame (model no. 1900, David Kopf Instruments, Tujunga, CA). An incision was made to expose the skull, including bregma, lambda, and the target sites. Stereotaxic coordinates were measured from Bregma and were based on The Mouse Brain in Stereotaxic Coordinates[66,67]. A hole was made above the target by thinning the skull using a small drill bit until only a very thin layer remained. An opening was then made using a microprobe, and the remaining thinned skull was gently pulled away. All animals were injected at each target with 500 nl of virus at a rate of ~150 nl/min using a Nanoject II microinjector (Drummond Scientific, Broomall, PA). Intraventricular injection of AAV-PHP.eB viruses was conducted by injecting 2 µl of virus into the lateral ventricle using a Nanoject II microinjectior. The glass pipettes had inner diameters between 10-20 µm.

Two weeks following AAV injection, animals were anesthetized and returned to the stereotaxic frame. An incision was made in the previous location to once again reveal the location of the injection sites. An LED light source (LED-64s, Amscope, Irvine, CA) was mounted to the surgical microscope and positioned 3-4 inches directly above the animal's skull. The amount of time the animal was exposed to light was varied by experiments. Small amounts of sterile PBS were periodically applied to the scalp and skull to prevent drying.

Two weeks following light exposure, animals were perfused with 4% paraformaldehyde (PFA). Brains were dissected and post-fixed in 4% PFA at room temperature for 3–6 h and then overnight at 4°C. Brains were then rinsed briefly with PBS and stored in PBS with 10% sucrose solution. Brains were then sectioned at a thickness of 100 µm while frozen on a sliding microtome (Leica SM2010 R, Nussloch, Germany). Brain sections were mounted on 1x3 in. Plus slides and coverslipped with Vectashield with DAPI (H-1500, Vector Laboratories, Burlingame, CA). Slides were then imaged using a 10x objective on a Leica TCS SP8 confocal microscope (Leica Microsystems, Buffalo Grove, IL).

For fMOST imaging, two weeks or longer following light exposure, animals were perfused with 4% paraformaldehyde (PFA). Brains were dissected and post-fixed in 4% PFA at room temperature for 3–6 h and then overnight at 4°C. Brains were then transferred to PBS with 0.1% sodium azide for storage at 4°C until embedding.

Surface/Cortical *In vivo* two-photon stimulation of DreV

A titanium head plate was attached to the skull of mice to allow positioning and restraint of the animal during imaging. The hole of the head plate was positioned over visual cortical areas, approximately 2.9 mm posterior and 2.7 mm lateral from Bregma. A 5 mm craniotomy was cut into the skull using a dental drill. The dura was then removed, and a multilayer glass coverslip was positioned above the craniotomy. The head plate and coverslips were secured using cyanoacrylate glue and metabond. After a period of at least one week, a dental drill was used to remove the cement and metabond holding the coverslip in place, and the coverslip was removed. A Dumont Nanoject II was then used to inject 500 nL of viruses into visual cortex. A new coverslip was placed and adhered. The area above the coverslip was blocked from light using a combination of dental cement and Kwik-cast, both mixed with black acrylic paint powder.

After at least 3 weeks following viral injection, the animal received two-photon laser stimulation. Under dark conditions, the Kwik-cast was removed and the animal's head plate was mounted in position. The injection area was identified by the presence of the EGFP labelled cells. Laser output was set to 900 nm to optimally induce recombination. A 600 x 600 µm area was stimulated at three depths (100 µm, 150 µm, and 200 µm) for 15 minutes each. After stimulation, black Kwik-cast was reapplied. Two weeks following stimulation, mice were perfused.

Deep brain stimulation/imaging *in vivo* experiments

Stereotaxic injections were made into Ai162-GC6s (Stock No. 031562, The Jackson Laboratory, Bar Harbour, ME, GCaMP6s reporter) mice with a 1:1 mixture of PHP.eB.iCreV and a reporter AAV (AAV5.CAG.tdTomato) into the striatum for one-photon stimulation. For two-photon stimulation, stereotaxic injections were made into C57BL/6NCrl (stock No. 027 Charles River, CA) mice, into two locations; PHP.eB.iCreV injected intracerebroventricular (ICV), and a 1:1 mixture of Cre-dependent virus (AAV5.Ef1a.DIO.mCherry) and a non-Cre-dependent virus (AAV5.hsyn.ChR2.eYFP) injected locally to the striatum. For all experiments, animals were anesthetized with isoflurane (5% induction, 1.5% maintenance) and placed on a stereotaxic frame (942, David Kopf Instruments, CA, USA). An incision was made to expose the skull, including bregma, lambda, and the target sites. Stereotaxic coordinates were measured from Bregma and were based on The Mouse Brain Atlas[66,67]. A full hole was made above the target. All animals were injected with 400 nl X 2 of virus mixture, at two dorsoventral positions, 300um apart, at a rate of ~80 nl/min using UltraMicroPump (UMP3-4, World Precision Instrument, Sarasota, FL), and an additional ICV injection of 2µl of PHP.eB.iCreV when mentioned (AP -0.6 mm, ML ± 1.15 mm, DV -2.1 and -1.8 mm, 1µl each). Following virus injection, an optical fiber with cut length of 5 mm and diameter of 400 µm (NA 0.48, Doric lenses, Quebec, QC, Canada) for one-photon stimulation, or 600nm GRIN lens (GLP-0673, Inscopix, Palo Alto, CA) for two-photon stimulation, was firmly mounted to a stereotaxic holder. The optical fiber/GRIN lens was then inserted to the striatum (AP +1.0 mm, ML ± 1.3 mm, DV -3.5 mm, from either left or right side) through a craniotomy, and positioned 300 µm above the deeper viral injection site. A thin layer of metabond was applied on the skull surface to secure the fiber. In addition, a thick layer of black dental cement was applied to secure fiber implant for 1P illumination, or to attach a ring around the GRIN lens to allow positioning and restraint of the animal during 2P illumination. At the end of GRIN lens implant surgery, the area above the GRIN lens was protected and blocked from light using a layer of Kwik-cast, a non-transparent adhesive, and a layer of Kwik-Sil (World Precision Instrument, Sarasota, FL), a stronger adhesive.

AAV5.hsyn.ChR2.eYFP (3.6 x 10^{12} GC/mL), AAV5.Ef1a.DIO.mCherry (4.8 x 10^{12} GC/mL) and AAV5.CAG.tdTomato (1.0 x 10^{13} GC/mL) were purchased at UNC Vector core. PHP.eB iCreV, (2.6 x 10^{13} GC/mL) was produced in house.

One-photon light activation: optical fiber

One week following AAV injection of 1:1 virus mixture of PHP.eB.iCreV and AAV5.CAG.tdTomato into GCaMP6s reporter mice, animals' baseline signals were recorded with a fiberphotometry rig for 10 minutes in the home cage. Fiberphotometry is a method for measuring population calcium dependent fluorescence from genetically defined cell types in deep brain structures using a single optical fiber for both excitation and emission in freely moving mice. Detailed description of the system can be found elsewhere[68]. After recording, mice were connected to a 447nm laser (Opto Engine LLC, UT) using a 200 µm optical fiber, illuminated with 5mW, 100ms pulses, 1Hz for 30 minutes (TTL-controlled by OTPG_4, Doric lenses, Quebec, QC, Canada), in the home-cage. A week following light exposure, fiberphotometry signal was recorded again for 10 minutes. Fiberphotometry peak detection was performed with MATLAB (R2018a), using 'findpeaks' function, using a prominence of 2.5. Mice were perfused 4 weeks after illumination.

Two-photon stimulation of CreV: GRIN lens

At least 3 weeks following ICV PHP.eB.iCreV injection and a 1:1 mixture of AAV5.Ef1a.DIO.mCherry and AAV5.hsyn.ChR2.eYFP injections into C57Bl/6N mice, animals received two-photon laser stimulation. The cast was removed and the animal's head ring was mounted in position under minimum light required, under light anesthesia (1- 1.5% isoflurane). Two photon illumination was carried by a tunable ultrafast laser system (Insight DS+, Spectra Physics, CA), coupled to a manually built two-photon microscope. Laser output was set to 900 nm to optimally induce recombination. A 500 x 500 µm area was stimulated at three depths (700 µm, 750 µm, and 800 µm, corresponding to Inscopix GRIN lens focusing properties) for 15 minutes each, at 0.3Hz scanning frequency. After stimulation, a small layer of Kwik-cast was reapplied, covered by a layer of Kwik-Sil. Two weeks following stimulation, the mice were perfused.

Immunohistochemistry

Animals were perfused with 4% paraformaldehyde (PFA). Brains were dissected and post-fixed in 4% PFA overnight at 4°C. Brains were then rinsed briefly with PBS and then sectioned at a thickness of 100 μm on a vibratome (VT1200 Leica Biosystems, IL, USA). Brain sections were incubated in a blocking solution, containing 1x PBS solution with 0.1% Triton X-100 and 10% normal donkey serum (NDS; Jackson ImmunoResearch, PA, USA) for at least an hour, washed, and further incubated with blocking buffer containing primary antibody (see below for details) at 4C overnight. Afterward, sections were thoroughly washed three times (15 min each) in 1x PBS and then transferred into the blocking solution with secondary antibody (see below for details) for 2h at room temperature. Finally, sections were again washed by 1x PBS solution four times (15 min each), mounted on glass microscope slides (Adhesion Superfrost Plus Glass Slides, #5075-Plus, Brain Research Laboratories, MA, USA), dried, and coverslipped with mounting media (Prolong Diamond, P36965, Thermo-Fischer, CA, USA). For primary antibody: chicken anti-mCherry (1:1000; ab205402, Abcam, Cambridge, UK) was used. For secondary antibody, anti-chicken Alexa Fluor 594 (1:500; 703-585-155, Jackson ImmunoResearch) was used.

Confocal microscopy imaging

Fluorescent images from brain tissue were acquired with an LSM 880 confocal microscope (Carl Zeiss, Jena, Germany). We used a 10x Plan Apochromat air objective (NA 0.45), 25x Plan Apochromat water immersion objective (NA 1.2) and three laser wavelengths (488 nm, 561 nm, and 633 nm). Image acquisition was controlled by Zen 2011 software (Zeiss), which also allowed automated tiling, and maximum intensity projection. Images were not further processed. Expression counts were done by summation of the values of the fluorescence within 1mmX1mm below the fiber/GRIN tip subtracted with the same area at the opposite hemisphere, line by line, and normalized to the maximal value.

fMOST imaging

All tissue preparation has been described previously[69]. Following fixation, each intact brain was rinsed three times (6 h for two washes and 12 h for the third wash) at 4°C in a 0.01 M PBS solution (Sigma-Aldrich Inc., St. Louis, US). Then the brain was subsequently dehydrated via immersion in a graded series of ethanol mixtures (50%, 70%, and 95% (vol/vol) ethanol solutions in distilled water) and the absolute ethanol solution three times for 2 h each at 4°C. After dehydration, the whole brain was impregnated with Lowicryl HM20 Resin Kits (Electron Microscopy Sciences, cat.no. 14340) by sequential immersions in 50, 75, 100 and 100% embedding medium in ethanol, 2 h each for the first three solutions and 72 h for the final solution. Finally, each whole brain was embedded in a gelatin capsule that had been filled with HM20 and polymerized at 50°C for 24 h.

The whole brain imaging is realized using a fluorescence microscopic optical sectioning tomography (fMOST) system. The basic structure of the imaging system is the combination of a wide-field upright epi-fluorescence microscopy with a mechanic sectioning system. This system runs in a wide-field block-face mode but updated with a new principle to get better image contrast and speed and thus enables high throughput imaging of the fluorescence protein labeled sample (manuscript in preparation). Each time we do a block-face fluorescence imaging across the whole coronal plane (X-Y axes), then remove the top layer (Z axis) by a diamond knife, and then expose next layer, and image again. The thickness of each layer is 1.0 micron. In each layer imaging, we used a strip scanning (X axis) model combined with a montage in Y axis to cover the whole coronal plane[70]. The fluorescence, collected using a microscope objective, passes a bandpass filter and is recorded with a TDI-CCD camera. We repeat these procedures across the whole sample volume to get the required dataset.

The objective used is 40X WI with numerical aperture (NA) 0.8 to provide a designed optical resolution (at 520 nm) of 0.37 μm in XY axes. The imaging gives a sample voxel of 0.30 x 0.30 x 1.0 μm to provide proper resolution to trace the neural process. The voxel size can be varied upon difference Objective. Other imaging parameters for GFP imaging include an excitation wavelength of 488 nm, and emission filter with passing band 510-550 nm.

Data availability

All relevant plasmids will be deposited to Addgene. Data are available from the corresponding author upon request.

ACKNOWLEDGMENTS

We are grateful to the Structured Science teams at the Allen Institute for their technical support in stereotaxic injections and mouse colony management. We thank Anton Maximov and Tom Wandless for providing the DHFR constructs. The work was funded by the Allen Institute for Brain Science, NIMH BRAIN Initiative grant RF1MH114106 to A.C., NSFC Science Fund for Creative Research Group of China (Grant No. 61421064) to H.G., Q.L. and S.Z., NIH Director's New Innovator award IDP20D017782 and NIH/NIA 1R01AG047664 to V.G., and Colvin divisional fellowship of Division of Biology and Biological Engineering, California Institute of Technology, to A.K. Immunohistochemistry experiments in Figure 8 were performed in the Biological Imaging Facility, with the support of the California Institute of Technology Beckman Institute and the Arnold and Mabel Beckman Foundation. The creation of Ai139 mouse line was supported by the NIH grant R01DA036909 to B.T. The authors wish to thank the Allen Institute founder, Paul G. Allen, for his vision, encouragement, and support.

AUTHOR CONTRIBUTIONS

A.C. conceptualized the light-inducible recombinase system. S.Y. performed cloning and characterization of the constructs as well as participated in image acquisition. B.O. performed all the surgeries and image acquisition. T.Z. Performed cloning. M.M. performed some of the surgeries and light stimulations. T.D. performed some of the initial cloning experiments. B.T. and H.Z. contributed to the generation of the Ai139 transgenic mice. H.G., Q.L. and S.Z. acquired fMOST data. X.K. and Y.W. performed Neurolucida reconstructions. V.G. and A.K. performed deep brain GRIN lens stimulation and imaging experiments. S.C. and P.B. performed 2P induced recombination experiments. A.C. and H.Z. designed and coordinated the study as well as wrote the manuscript, with inputs from all coauthors.

COMPETING FINANCIAL INTERESTS

The authors declare no competing financial interests.

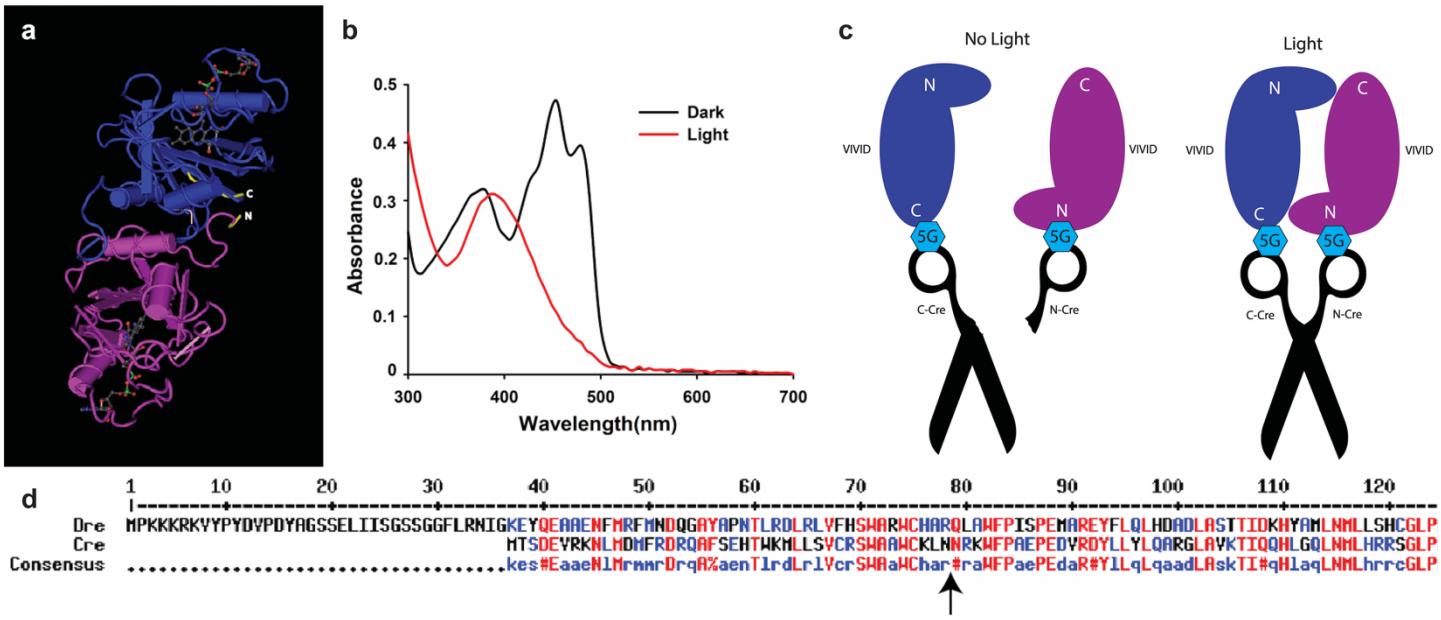

Figure 1. Design of the VVD-Cre (CreV) and VVD-Dre (DreV) systems. (**a**) Crystal structure of the Vivid (VVD) protein (adapted from REF[37]). The N terminus (yellow) of one VVD domain (magenta) comes in close proximity to the C terminus (yellow) of the second VVD domain (blue) in dimer form. (**b**) Both monomer and dimer of VVD have a sharp cutoff in absorption above 520 nm, which allows longer wavelengths to be utilized without interference (adapted from REF[19]). (**c**) Design of VVD-Cre. Cre is split into two halves: N-Cre and C-Cre. Each half is linked to a VVD domain via a penta-glycine linker (light blue 5G) to maximize flexibility. Upon light induced dimerization of the VVD domains, the two halves of Cre are brought together and Cre activity is restored (right panel). (**d**) The consensus between the amino acid sequences of Cre and Dre recombinases. Multiple sequence alignment using Multalin reveals the homology between the two sequences. Using this information, we split Dre at the arginine (R) to glutamine (N) transition marked with the arrow.

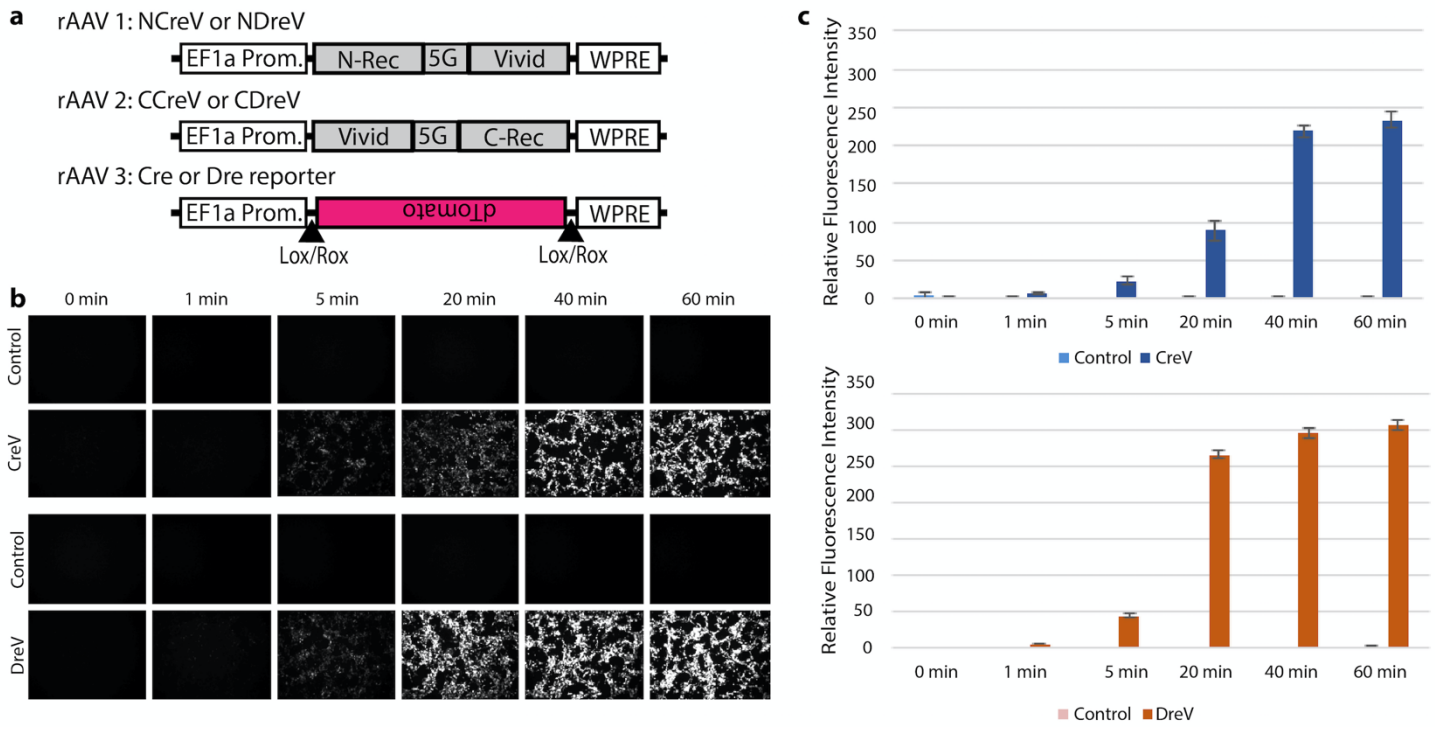

Figure 2. Light induced CreV and DreV recombination in HEK293T cells. (**a**) Schematic of the rAAV constructs. Rec (recombinase) represents either Cre or Dre. CreV (NCreV + CCreV) or DreV (NDreV + CDreV) fusion constructs were co-transfected with a Cre- or Dre-dependent red fluorescent (dTomato) reporter. (**b**) Results of different durations of light induction at 458 nm wavelength of a 1.3 mW/mm^2 LED light source were documented at 48 hours post induction, or dark as controls. (**c**) Quantification of relative fluorescence intensity of the dTomato reporter shows robust light-induced recombination for both CreV and DreV. Each experiment is represented by 4 replicates and error bars indicate standard deviations.

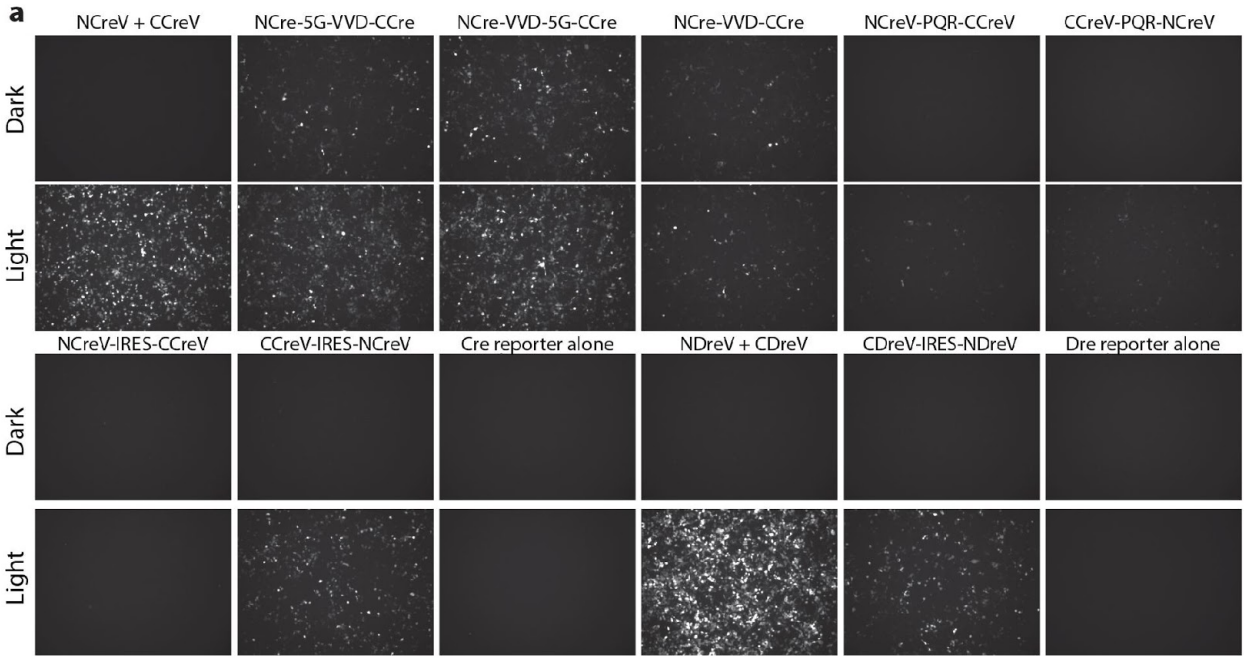

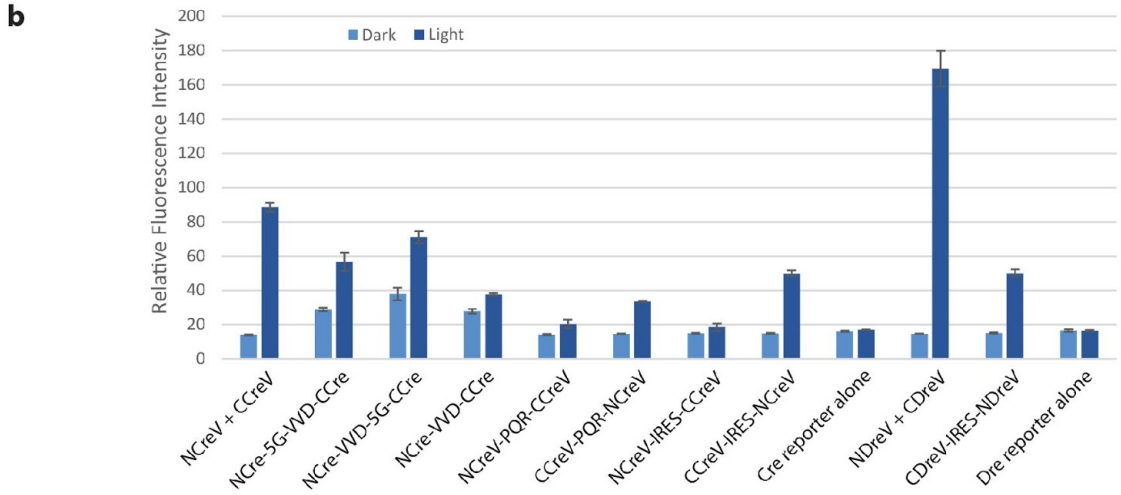

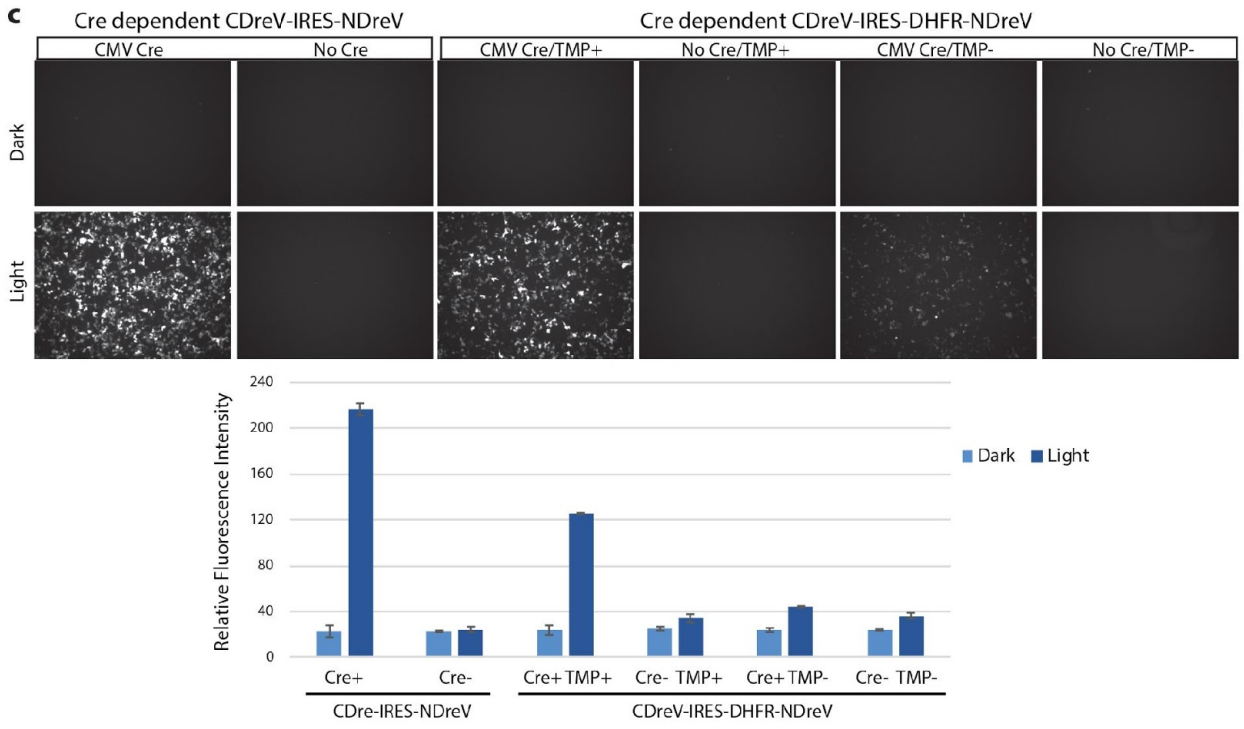

Figure 3. Tandem co-expression constructs for regular and drug-inducible RecV system. (**a**) Representative images from CreV and DreV co-expression variants (**Supplementary Fig. 1**) transfected in HEK293T cells. Top panels are dark control conditions. Bottom panels are images taken 48 hours after 20 minutes of light induction. (**b**) Relative fluorescence intensity of Cre dependent dTomato and Dre dependent dTomato reporters 48 hours after 20 minutes of light induction for different co-expression constructs. The N- and the C-termini of the CreV recombinase were combined using a variety of approaches. In the first one, the NCreV and CCreV constructs were mixed together. The next three contain NCre linked with VVD and CCre all within the same open reading frame, with or without a 5G linker. The fifth and sixth constructs contain both NCreV and CCreV linked by the ribosome skipping peptide PQR. The next two constructs have NCreV and CCreV linked by IRES sequence instead of PQR. Controls are represented by reporters alone. (**c**) Comparison of the light-inducible recombination mediated by Cre-dependent DreV and DHFR-DreV constructs in the absence and presence of Cre and/or TMP. HEK293T cells were co-transfected with the EF1a-Frex-dTomato Dre reporter and conditional RecV constructs, with or without pCMV-Cre (a Cre expressing plasmid). Cells transfected with DHFR-DreV were divided into the TMP+ and TMP- groups, which underwent medium exchange 6 hr after transfection, either to fresh medium containing 10 μM of TMP or that containing the same volume of the solvent. Top panels are dark control conditions. Bottom panels are images taken 48 hours after 20 minutes of light induction. Significant light-mediated activation of the Dre-dependent reporter was only observed for DreV in the presence of Cre, and for DHFR-DreV in the presence of Cre and TMP. Relative fluorescence intensities were calculated from 4 replicates in all cases.

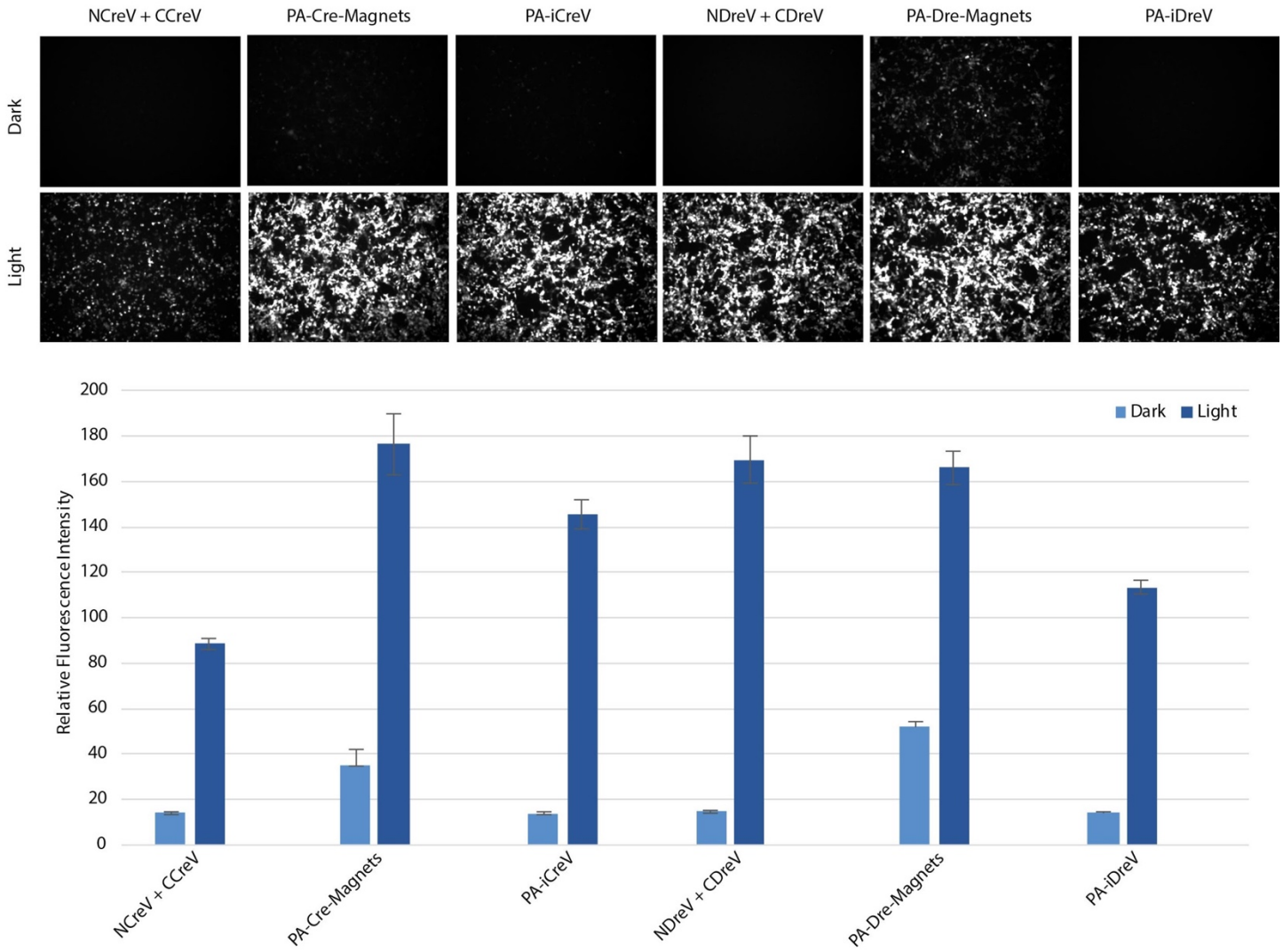

Figure 4. Comparison of the light-inducible recombination mediated by improved CreV and DreV. HEK293T cells were co-transfected with the appropriate Cre-dependent dTomato or Dre-dependent dTomato reporter, and various recombinase constructs, including mixed NRecV and CRecV, NRec-Magnets-NLS-P2A-NLS-Magnets-CRec (PA-Cre-Magnets and PA-Dre-Magnets), and NRec-VVD-NLS-P2A-NLS-VVD-CRec (PA-iCreV and PA-iDreV). Top panels are dark control conditions. Bottom panels are images taken 48 hours after 20 minutes of light induction. Relative fluorescence intensities were calculated from 4 replicates.

a

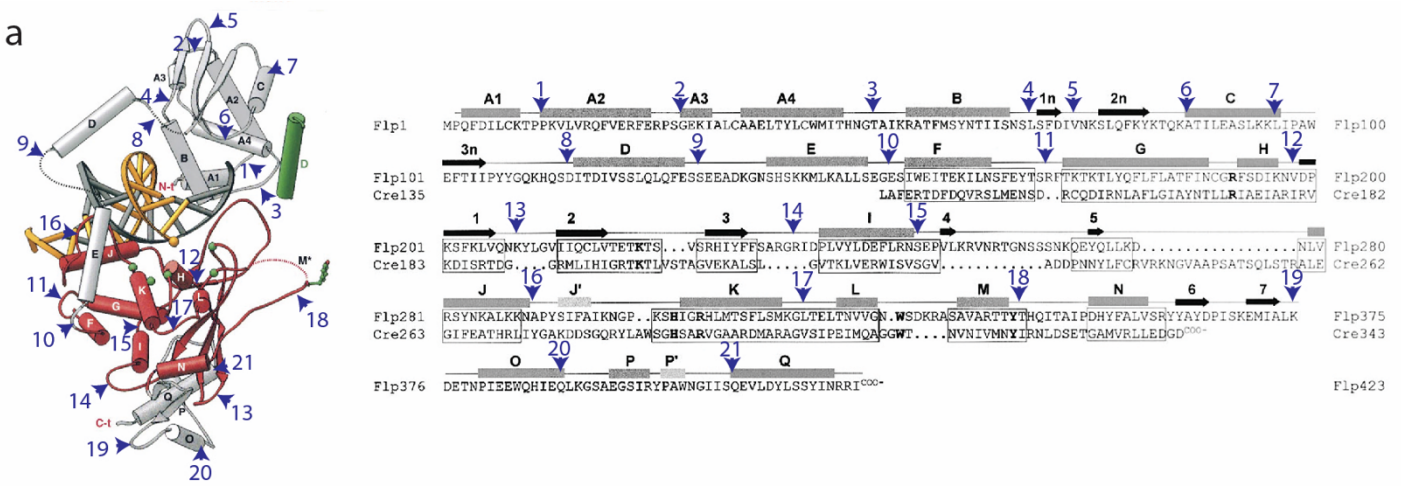

b

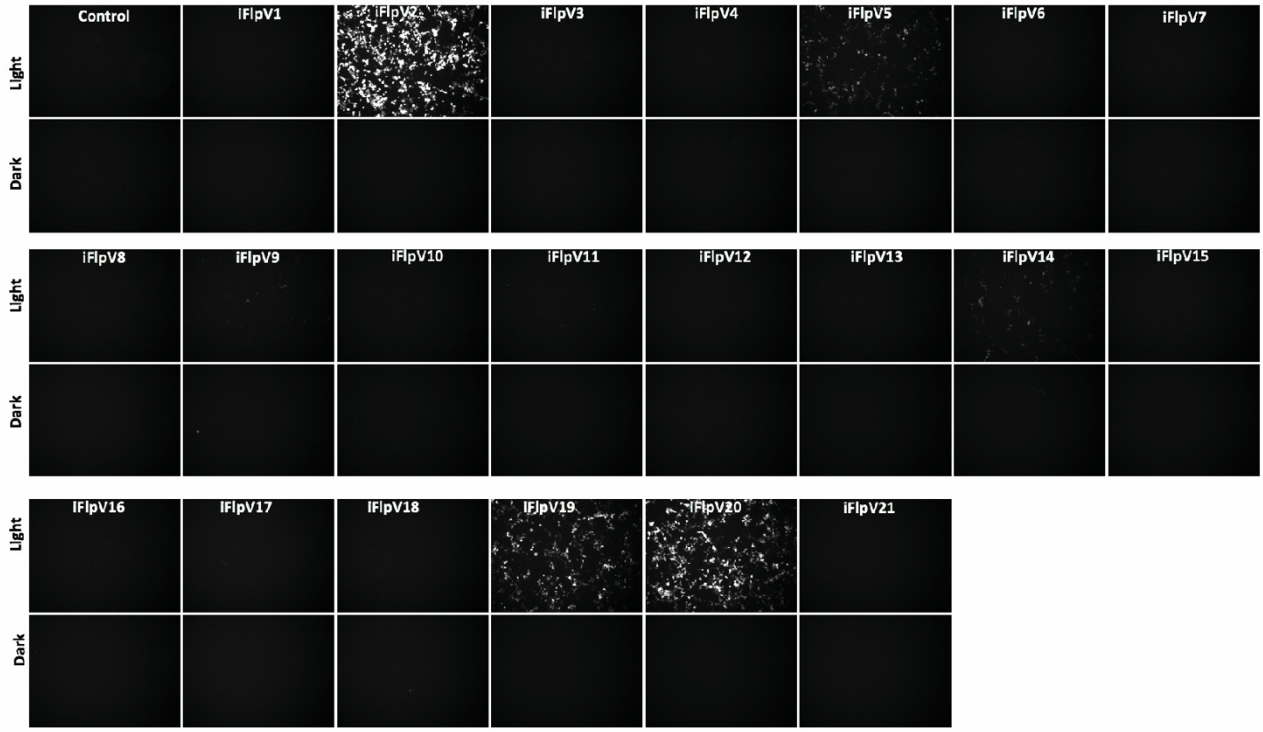

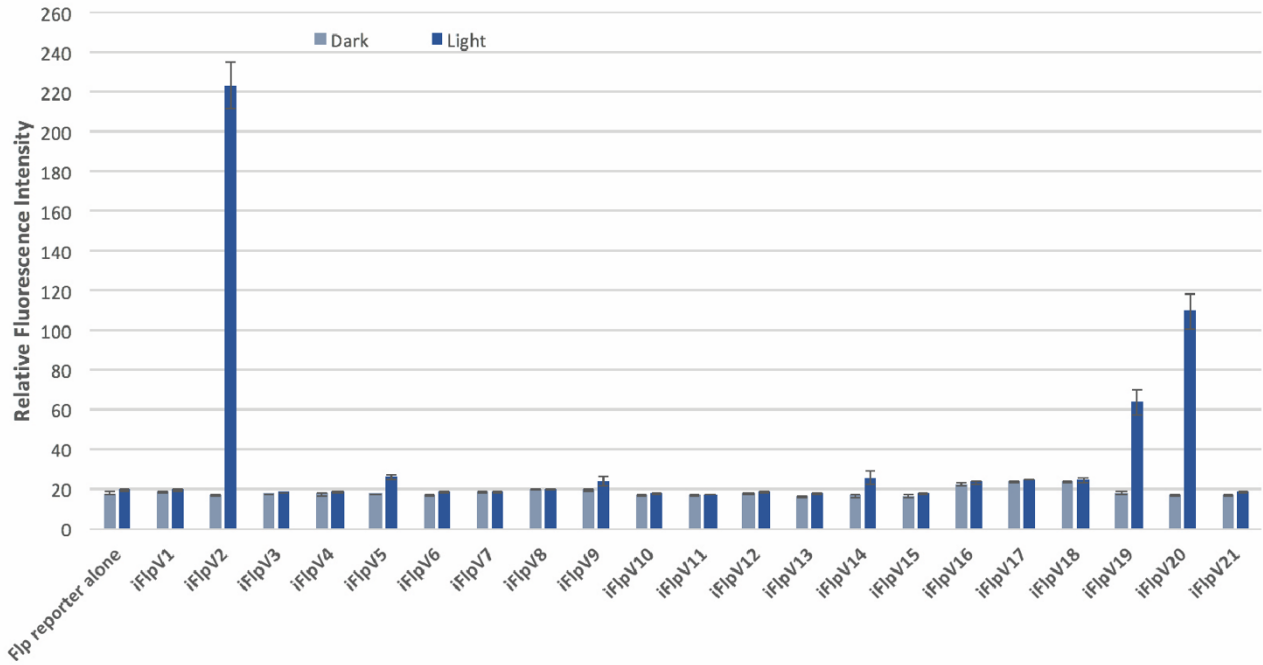

Figure 5. Generation of a novel light inducible Flp recombinase. (**a**) 21 different PA-iCreV based iFlpV constructs were generated by varying the splitting locations of the Flp open reading frame (**Supplementary Fig. 4**) (crystal structure and sequence alignment from REF[48]). (**b**) The expression plasmids containing these constructs were co-transfected into HEK293T cells with a Flp-dependent dTomato reporter (**Supplementary Fig. 1**), and stimulated with either 20 minutes of light or left in dark (n = 4 per case). 48 hours after light and dark treatments cells were imaged and relative fluorescence intensities were graphed.

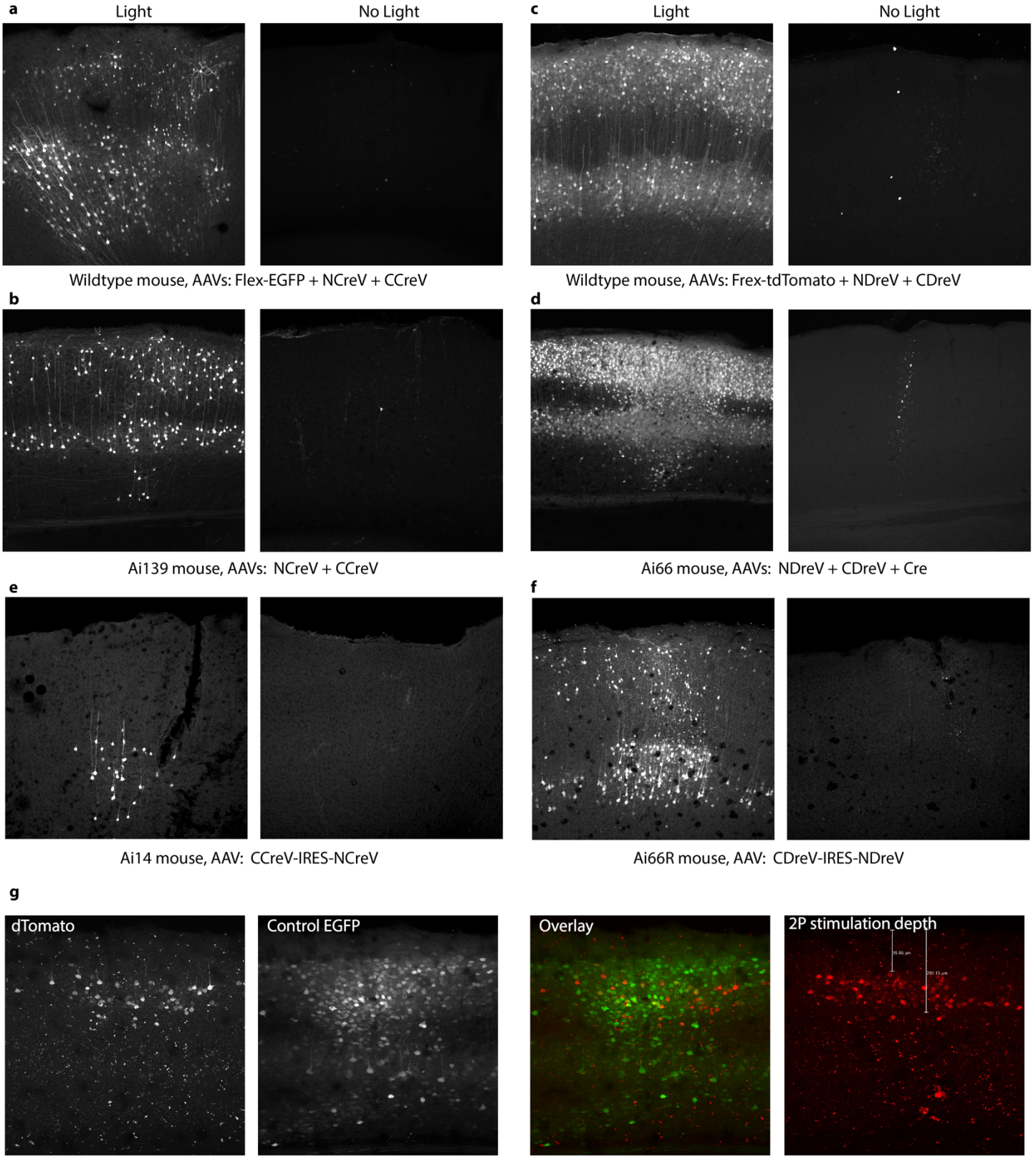

Figure 6. ***In vivo*** **light induced recombination using the RecV system**. (**a**) Wild-type mice were injected with a 1:1:1 mixture of the AAV-EF1α-NCreV, AAV-EF1α-CCreV, and Cre-dependent Flex-EGFP reporter AAV viruses. Injections were made into the visual cortex, and two weeks post-injection the entire skull and bore holes (site of craniotomy) of individual mice was exposed for 30 min to 340 mW/m^2 light (left panel). No light was applied to control mice with virus injections (right panel). Native fluorescence was analyzed in brain sections two

weeks post-light stimulation. Same procedure applies to panels **b-f** (n = 3 mice each for a-d or 2 for e-f). (**b**) Ai139 Cre reporter mice were injected with a 1:1 mixture of the AAV-EF1α-NCreV and AAV-EF1α-CCreV viruses. (**c**) Wild-type mice were injected with a 1:1:1 mixture of the AAV-EF1α-NDreV, AAV-EF1α-CDreV, and Dre-dependent Frex-dTomato reporter AAV viruses. (**d**) Ai66 (a Cre and Dre dependent tdTomato-expressing line[51]) mice were injected with a 1:1:1 mixture of the AAV-EF1α-NDreV, AAV-EF1α-CDreV, and AAV-EF1a-Cre viruses. (**e**) Ai14 mice (a Cre dependent tdTomato expressing mouse line) were injected with a single CCreV-IRES-NCreV expressing AAV. (**f**) Ai66R mice (a Dre dependent tdTomato expressing mouse line) were injected with a single CDreV-IRES-NDreV AAV. In all cases, the center of the injection for the dark condition is marked by debris autofluorescence and neuronal morphology is undetectable even with increased exposure. (**g**) A wild-type mouse was headpost implanted and injected with a 1:1:1:1 mixture of AAV-EF1a-NDreV, AAV-EF1a-CDreV, Dre-dependent Frex-dTomato reporter AAV, and human Synapsin promoter-driven EGFP AAV viruses. 2P light was applied through the cranial window to three 600 x 600 μm planes with 100, 150 and 200 μm depths. 2P induced recombination (as shown by dTomato-labeled cells) can be detected in layer 2/3 whereas control EGFP virus labels non-selectively across all cortical layers.

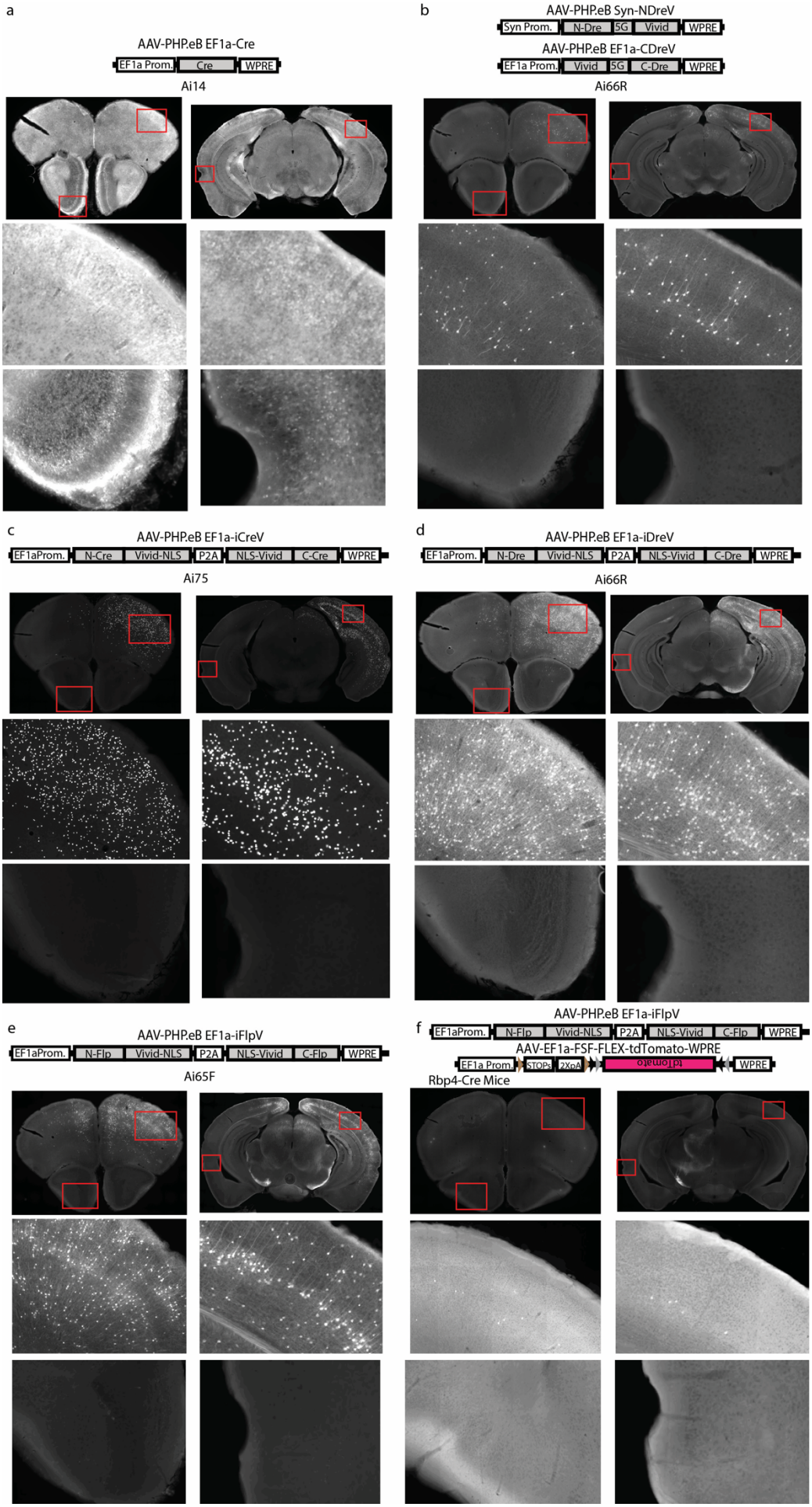

Figure 7. Whole brain infection and light mediated recombination using AAV-PHP.eB RecV viruses. Various reporter mice (n = 2 per case) each received intracerebroventricular (ICV) injection of 2 µl of the following rAAVs through the right hemisphere. (**a**) Cre-dependent tdTomato-expressing Ai14 mice were injected with AAV-PHP.eB EF1a-Cre virus. (**b**) Dre-dependent tdTomato-expressing Ai66R mice were injected with a 1:1 mixture of AAV-PHP.eB Syn-NDreV and AAV-PHP.eB EF1a-CDreV. (**c**) Cre-dependent nls-tdTomato expressing Ai75 mice were injected with AAV-PHP.eB EF1a-iCreV. (**d**) Ai66R mice were injected with AAV-PHP.eB EF1a-iDreV. (**e**) Flp-dependent tdTomato-expressing Ai65F mice were injected with AAV-PHP.eB EF1a iFlpV. (**f**) Layer 5 pyramidal neuron class specific Rbp4-Cre mice were injected with a mixture of AAV-PHP.eB EF1a iFlpV and AAV-PHP.eB EF1a-FSF-FLEX-tdTomato. All *in vivo* light activation was applied through the skull on the left hemisphere contralateral to the ICV injection sites. Experimental mice were treated with light 2 weeks post virus injection and sacrificed 2 weeks post light stimulation. Two coronal planes are shown for each injection (top row) with enlarged views (lower two rows) for areas indicated by the red boxes.

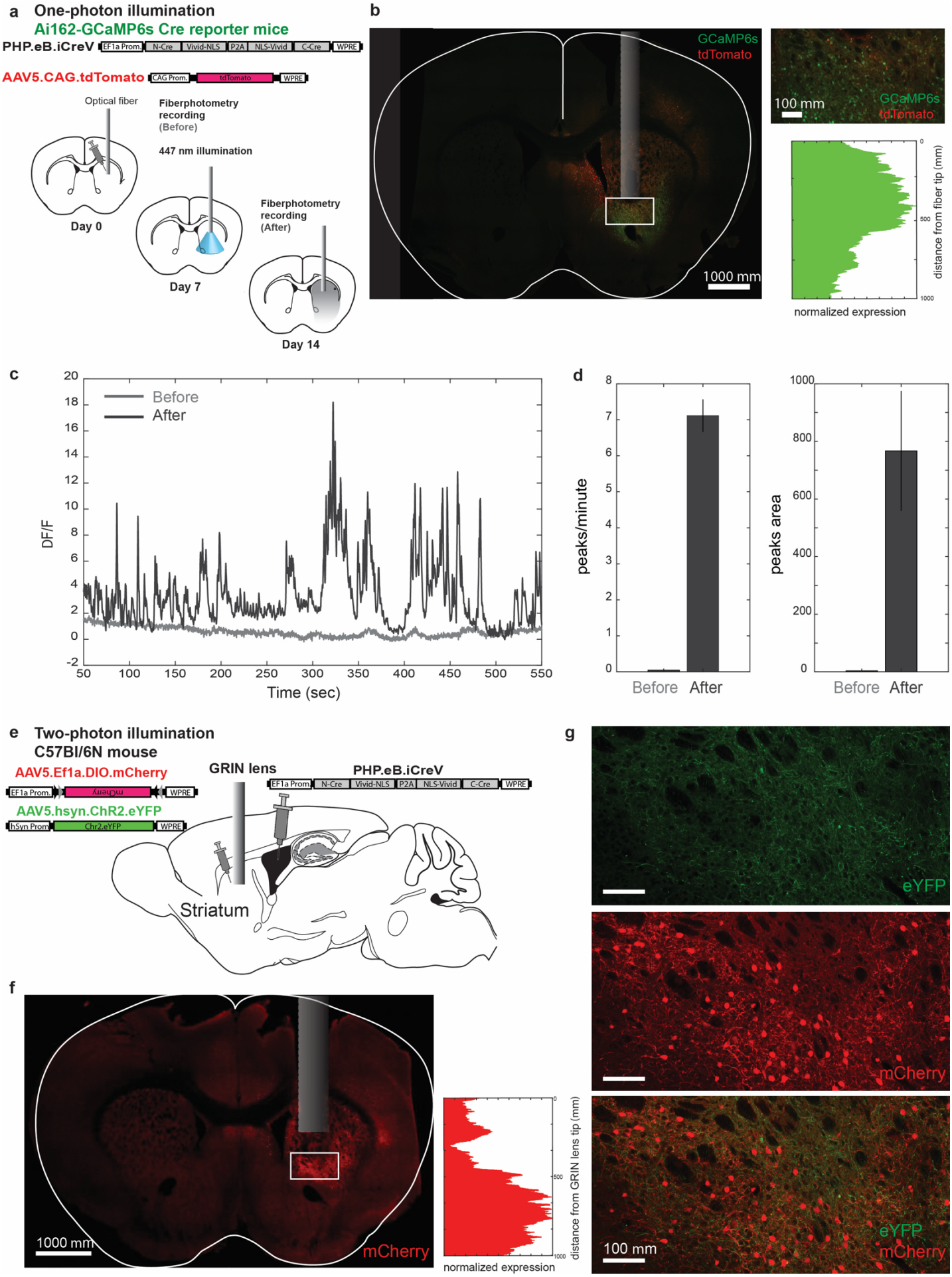

Figure 8. Deep brain illumination and application of iCreV. (**a-d**) One-photon illumination. (**a**) Virus application scheme and implant for one-photon illumination and GCaMP6s recording. GCaMP6s reporter mice were locally injected with 1:1 mixture of PHP.eB.iCreV and AAV5.CAG.tdTomato and implanted with 400 µm optical fiber. After 7 days, fiberphotometry signal was recorded as baseline activity, and one-photon illumination was performed by a 447nm laser using a 200 µm fiber, 5mW, 100ms pulses, 1Hz for 30 minutes. At day 14 fiberphotometry signal was measured. (**b**) Immunohistochemistry, representative, showing broad expression of tdTomato, and local and defined expression of GCaMP6s, just under the fiber tip, due to iCreV illumination and GCaMP6s expression. (**c**) Fiberphotometry activity in the striatum, caused by Cre recombination and induction of GCaMP6s due to illumination. 'Before' represents baseline activity before illumination, 'After' represents GCaMP6s activity a week after illumination. (**d**) Peaks/minutes and peak area of ΔF/F, before and after illumination (2 mice, 1 trial each). (**e-g**) Two-photon illumination at depth. (**e**) Virus application scheme and GRIN lens implant. C57Bl/6N mouse was injected with PHP.eB.iCreV into the ICV and with a 1:1 mixture of AAV5.Ef1a.DIO.mCherry and AAV5.hsyn.ChR2.eYFP in the striatum, and implanted with a GRIN lens. After 3 weeks, deep illumination was applied by two-photon microscope, 900nm, 90mW, under light anesthesia (1.5% isoflurane), at three depths, scanned 15 minutes each. (**f**) Immunohistochemistry, showing AAV5.Ef1a.DIO.mCherry expression due to illumination. Gray box shows the lens path. (**g**) Magnified area of white box at (f), showing mCherry expression due to illumination of iCreV. eYFP signal shows non-Cre dependent virus expression of ChR2.

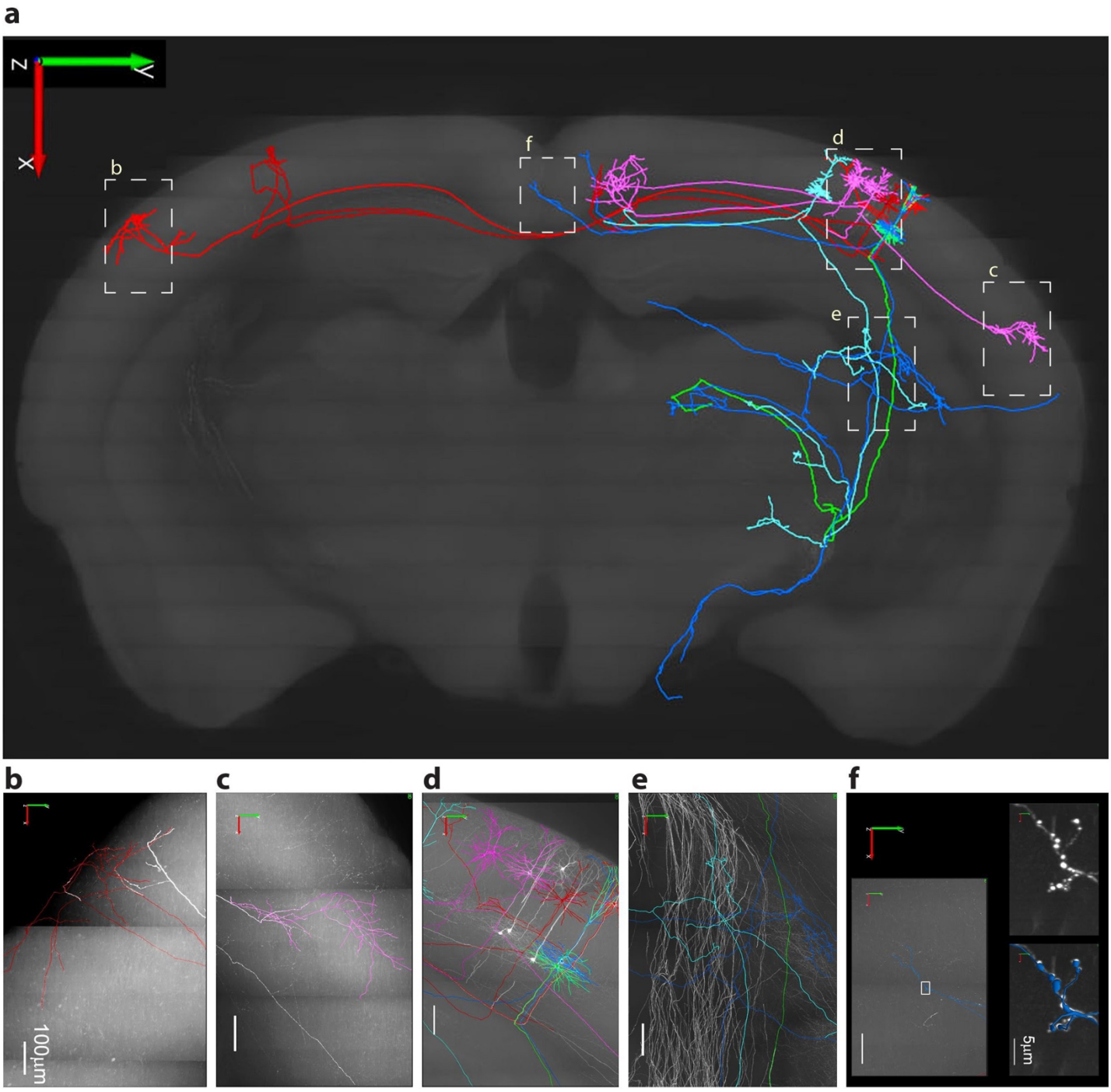

Figure 9. Cortical pyramidal cells (PCs) labeled with CreV and reconstructed at whole brain level. (**a**) Reconstructed 8 PCs in mouse barrel cortex include 3 layer 2/3 PCs (in pink) with ipsilateral cortico-cortical projections, 2 layer 2/3 PCs (in red) with contralateral cortico-cortical projections, and 3 layer 5 thick tufted PCs (1 in green, 1 in blue, 1 in light blue) with ipsilateral cortico-subcortical projections. Local axonal clusters are incomplete because the labeling at the somata region is still too dense in this brain for tracing fine axonal branches. The 8 reconstructed PCs are superimposed onto a coronal brain plane located 5201-5400 μm posterior to the olfactory bulb. (**b-f**) Enlarged views of areas outlined by dashed boxes in **a**, with reconstructions (in colors) superimposed on original images with GFP fluorescence in white. In **f**, the two panels on the right (without or with reconstructions in blue) are enlarged views of the boxed area in the left panel, showing the high-resolution details of a segment of axon with enlarged boutons clearly visible. The whole brain image stack (composed of 12089 images, resolution of XYZ, 0.3 x 0.3 x 1 μm) was obtained using fluorescence micro-optical sectioning tomography system (fMOST). 3D reconstruction was done manually with Neurolucida 360 (NL360).

pCDNA3.1 test plasmids:

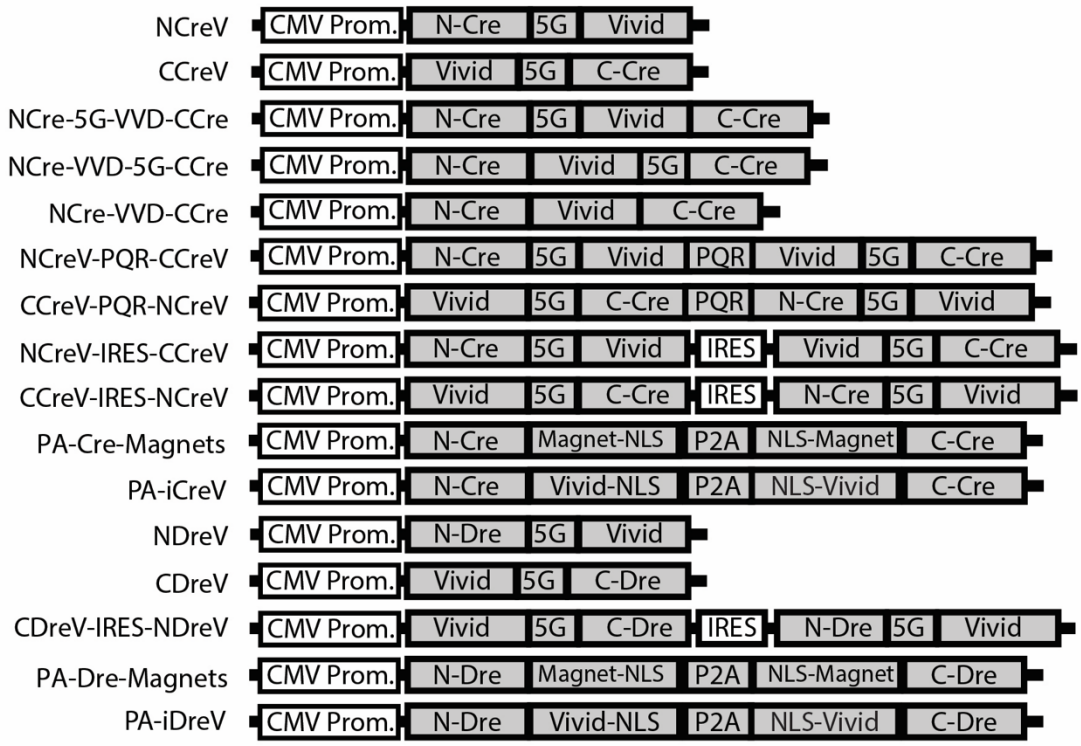

rAAV constructs:

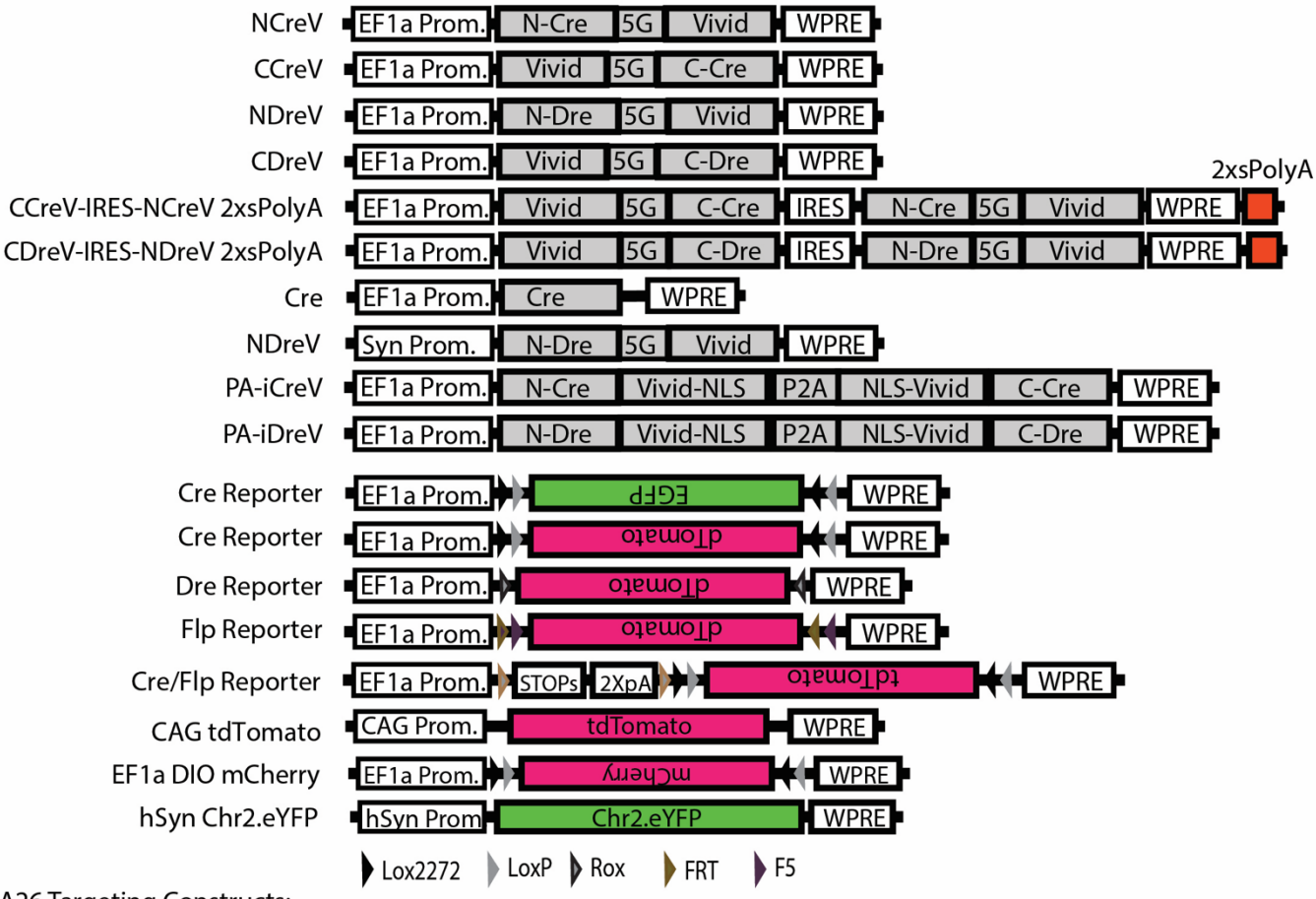

ROSA26 Targeting Constructs:

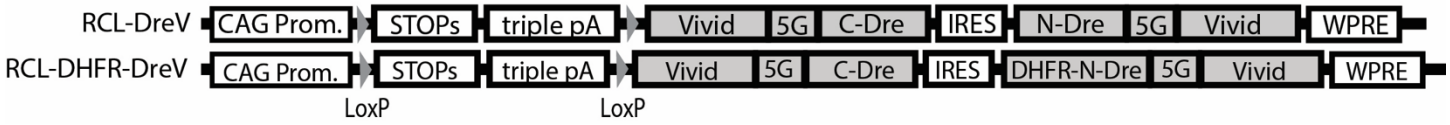

Supplementary Figure 1. Schematic diagram of DNA constructs generated for the study.

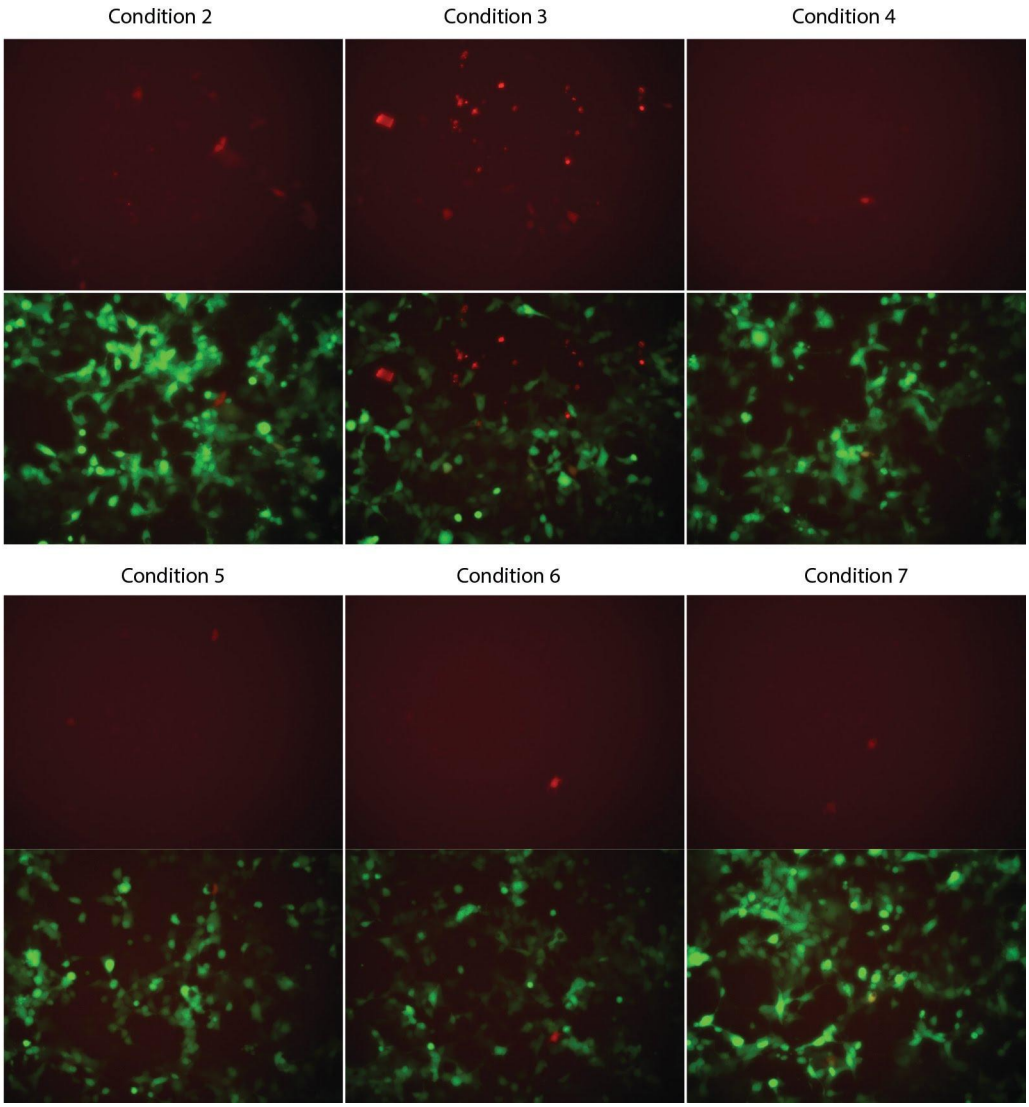

Supplementary Figure 2. *In vitro* two-photon stimulation of DreV. HEK293T cells were co- transfected with EF1a-EGFP, EF1a-Frex-dTomato, EF1a-NDreV, and EF1a-CDreV plasmids. Two-photon activation was conducted at 48 hr after transfection at various conditions, and reporter expression was observed 36 hr post stimulation. Two-photon activation conditions were as follows: λ = 900 nm, 90 mW, 1 ms/line (512 lines), 200 μm x 200 μm scan area, and duration of: 1) 3 mins (data not shown due to no signal), 2) 6 mins, 3) 9 mins, 4) 12 mins, 5) 12 mins (repeat), 6) 15 mins. In condition 7 randomly selected single cells were scanned in 5 areas, 36 x 36 μm each, separated by 40 μm roughly in a straight line across the plate with a duration of 1-10 seconds per area.

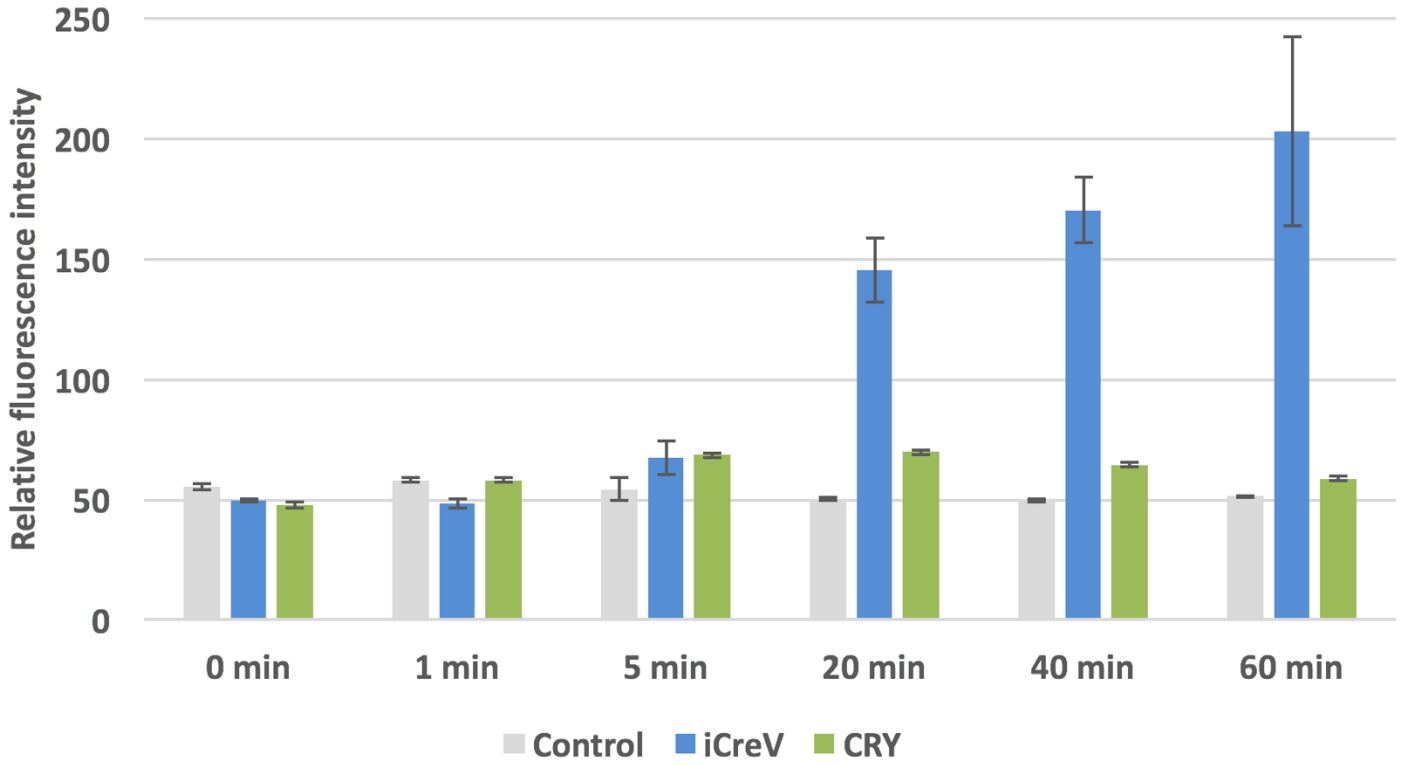

Supplementary Figure 3. The iCreV (PA-iCreV) system is superior over improved CRY2 based light inducible Cre recombination system. HEK293T cells were transiently transfected with dTomato reporter construct along with either PA-iCreV or improved CRY2/CIB1 based construct. 48 hours after various durations of light stimulation average fluorescence values were quantified with 4 replicates per condition.

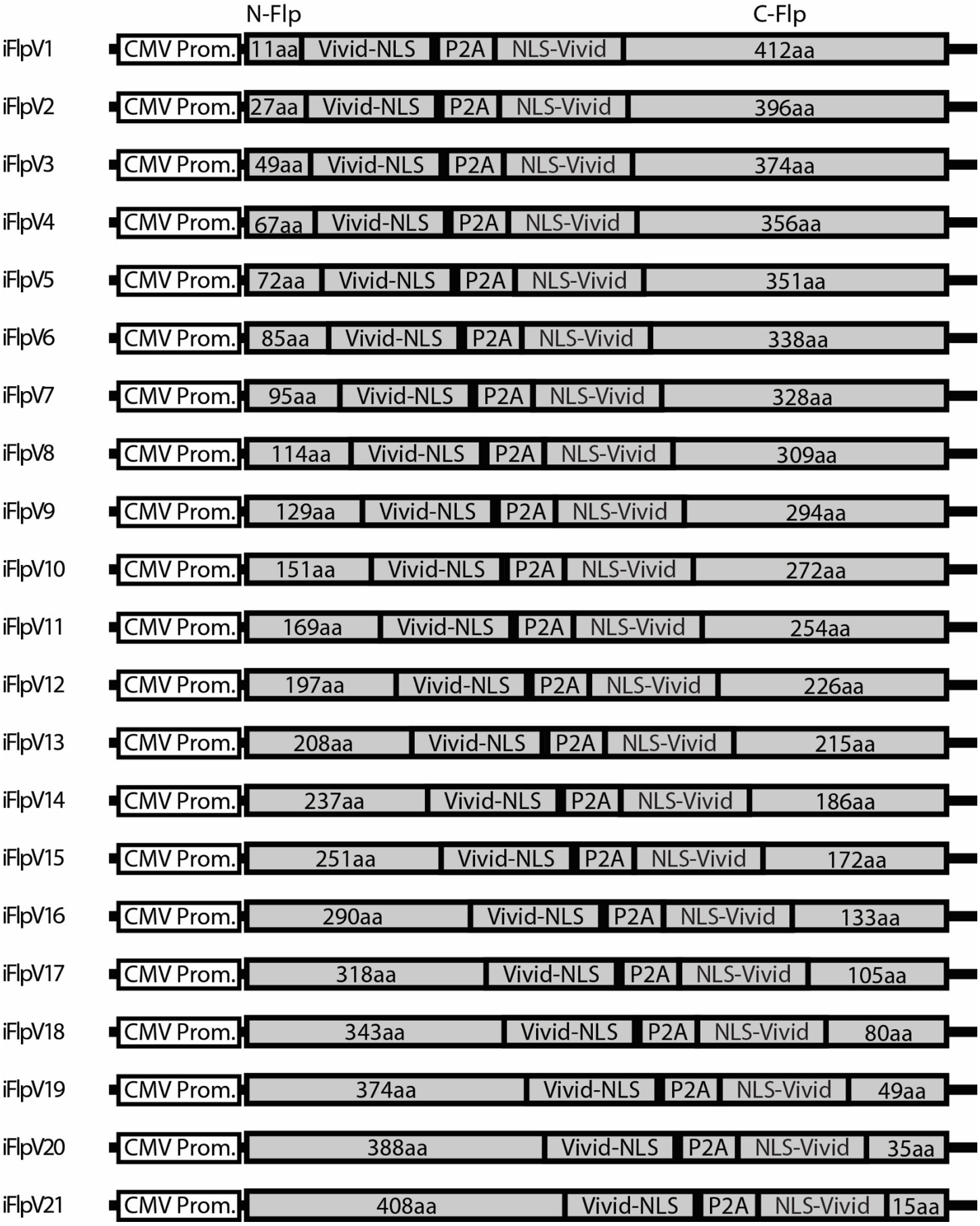

Supplementary Figure 4. Schematic diagram of iFlpV DNA constructs generated for the study.

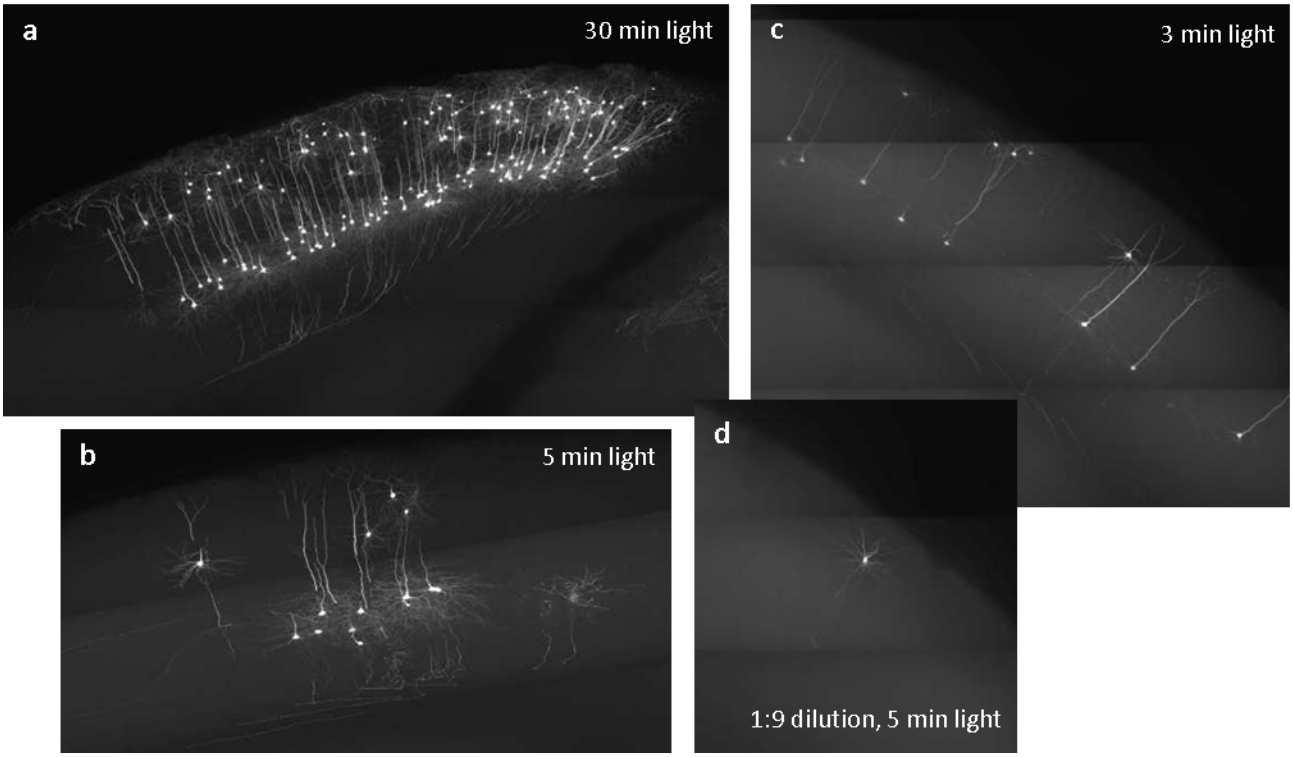

Supplementary Figure 5. Lower dose of CreV viruses and shorter duration of light induction leads to sparse and strong labeling of individual neurons. Ai139 Cre-dependent EGFP-expressing transgenic mice were injected with the 1:1 mixture of NCreV and CCreV rAAVs in different dilutions in the visual or somatosensory cortex. Two weeks after injection, various durations of light were applied across the skull at the injection sites. Two weeks post light induction, the brains were collected for fMOST imaging. Shown here are examples for the number of neurons labeled at the injection sites: (**a**) injection using undiluted viral solution, 30 minutes of light exposure; (**b**) injection using undiluted viral solution, 5 minutes of light; (**c**) injection using undiluted viral solution, 3 minutes of light; (**d**) injection using 1:9 dilution of viral solution, 5 minutes of light. Images are maximum projections of 100 consecutive fMOST images (each 1 μm-thick), thus equivalent to 100 μm-thick sections.

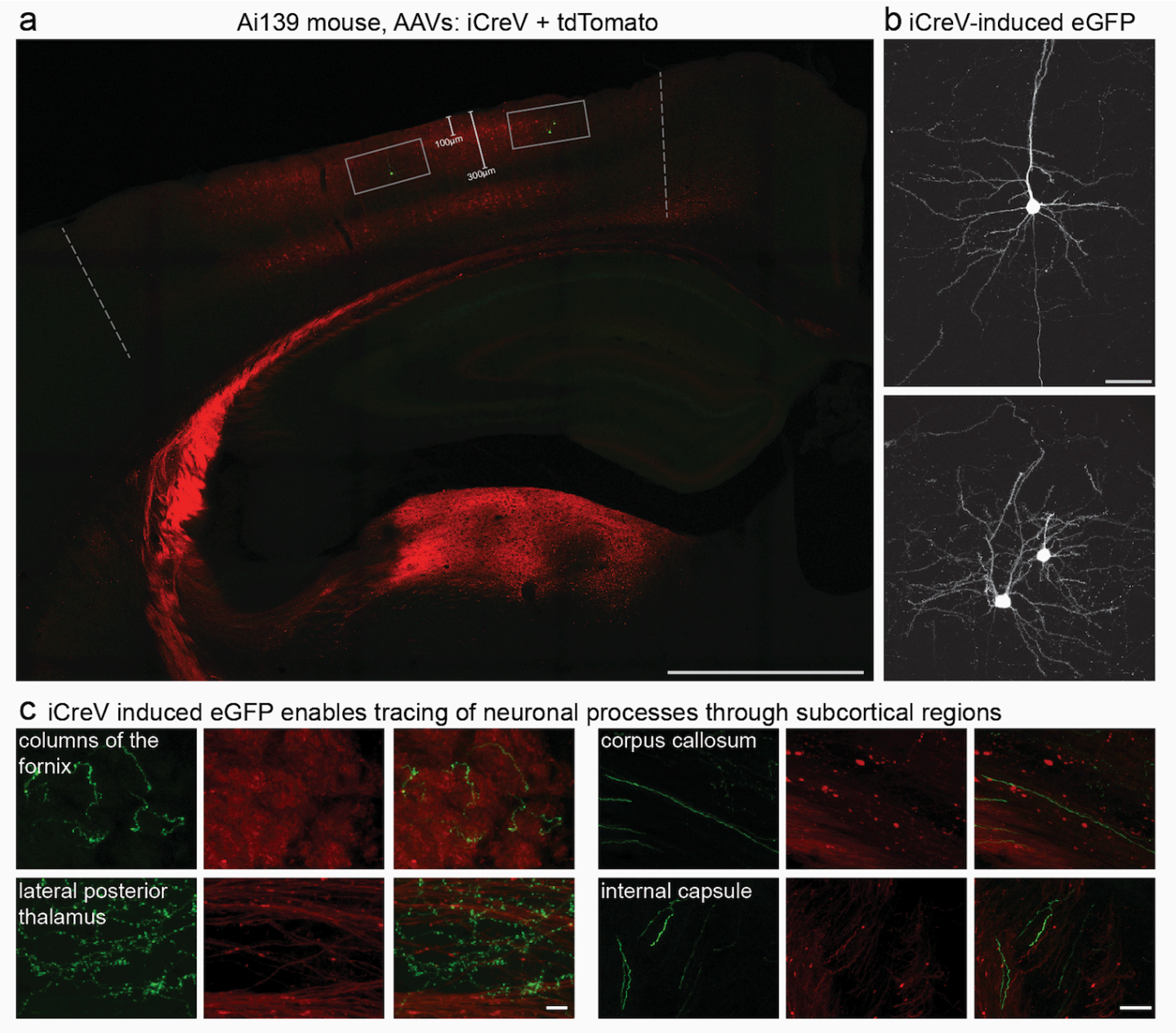

Supplementary Figure 6. In vivo two-photon stimulation and sparse recombination using iCreV. **(a)** Ai139 mice received single stereotaxic injections of a 1:5 mixture of EF1a-iCreV:EF1a-tdTomato into VISp. A glass cranial window and headplate were fitted over the injected region and temporarily covered with Kwik-cast mixed with black powder paint until two-photon stimulation. Gray dotted lines mark edges of the cranial window region. Two to three weeks post-injection, mice were head-fixed while walking on a stable platform, kwik-cast over the cranial window was removed, and discrete 400μm x 400μm regions of layer 2/3, approximately 150-250μm below the pial surface (gray boxes), were stimulated at λ = 910nm for 15 minutes each. Following stimulation, the window was recovered with kwik-cast mixed with black paint and animals were returned to their home cage. Two weeks later, animals were perfused. Scale bar is 1mm. **(b)** High magnification images of egfp-filled neurons within stimulated regions in (a). Two-photon stimulation of iCreV induced sparse eGFP expression within each region, visualizing individual neurons and their associated processes. Scale bar is 50μm. (c) Individual neuronal processes (right panels) and terminations (left panels) are traceable through multiple subcortical regions, enabling brain-wide morphological reconstructions of individual neurons. Scale bars are 10μm (left) and 30μm (right).

REFERENCES

1 Huang, Z. J. & Zeng, H. Genetic approaches to neural circuits in the mouse. *Annu Rev Neurosci* **36**, 183-215, doi:10.1146/annurev-neuro-062012-170307 (2013).

2 Nagy, A. Cre recombinase: the universal reagent for genome tailoring. *Genesis* **26**, 99-109 (2000).

3 Branda, C. S. & Dymecki, S. M. Talking about a revolution: The impact of site-specific recombinases on genetic analyses in mice. *Dev Cell* **6**, 7-28 (2004).

4 Glaser, S., Anastassiadis, K. & Stewart, A. F. Current issues in mouse genome engineering. *Nat Genet* **37**, 1187-1193, doi:10.1038/ng1668 (2005).

5 Velez-Fort, M. *et al.* The stimulus selectivity and connectivity of layer six principal cells reveals cortical microcircuits underlying visual processing. *Neuron* **83**, 1431-1443, doi:10.1016/j.neuron.2014.08.001 (2014).

6 Marshel, J. H., Mori, T., Nielsen, K. J. & Callaway, E. M. Targeting Single Neuronal Networks for Gene Expression and Cell Labeling In Vivo. *Neuron* **67**, 562-574 (2010).

7 Rompani, S. B. *et al.* Different Modes of Visual Integration in the Lateral Geniculate Nucleus Revealed by Single-Cell-Initiated Transsynaptic Tracing. *Neuron* **93**, 767-776 e766, doi:10.1016/j.neuron.2017.01.028 (2017).

8 Luo, L. Fly MARCM and mouse MADM: genetic methods of labeling and manipulating single neurons. *Brain Res Rev* **55**, 220-227, doi:10.1016/j.brainresrev.2007.01.012 (2007).

9 Denk, W., Strickler, J. H. & Webb, W. W. Two-photon laser scanning fluorescence microscopy. *Science* **248**, 73-76 (1990).

10 Shimizu-Sato, S., Huq, E., Tepperman, J. M. & Quail, P. H. A light-switchable gene promoter system. *Nat Biotechnol* **20**, 1041-1044, doi:10.1038/nbt734 (2002).

11 Levskaya, A., Weiner, O. D., Lim, W. A. & Voigt, C. A. Spatiotemporal control of cell signalling using a light-switchable protein interaction. *Nature* **461**, 997-1001, doi:10.1038/nature08446 (2009).

12 Kawano, F., Suzuki, H., Furuya, A. & Sato, M. Engineered pairs of distinct photoswitches for optogenetic control of cellular proteins. *Nat Commun* **6**, 6256, doi:10.1038/ncomms7256 (2015).

13 Muller, K. *et al.* A red/far-red light-responsive bi-stable toggle switch to control gene expression in mammalian cells. *Nucleic Acids Res* **41**, e77, doi:10.1093/nar/gkt002 (2013).

14 Lungu, O. I. *et al.* Designing photoswitchable peptides using the AsLOV2 domain. *Chem Biol* **19**, 507-517, doi:10.1016/j.chembiol.2012.02.006 (2012).

15 Crefcoeur, R. P., Yin, R., Ulm, R. & Halazonetis, T. D. Ultraviolet-B-mediated induction of protein-protein interactions in mammalian cells. *Nat Commun* **4**, 1779, doi:10.1038/ncomms2800 (2013).

16 Strickland, D. *et al.* TULIPs: tunable, light-controlled interacting protein tags for cell biology. *Nature methods* **9**, 379-384, doi:10.1038/nmeth.1904 (2012).

17 Kennedy, M. J. *et al.* Rapid blue-light-mediated induction of protein interactions in living cells. *Nature methods* **7**, 973-975, doi:10.1038/nmeth.1524 (2010).

18 Motta-Mena, L. B. *et al.* An optogenetic gene expression system with rapid activation and deactivation kinetics. *Nat Chem Biol* **10**, 196-202, doi:10.1038/nchembio.1430 (2014).

19 Wang, X., Chen, X. & Yang, Y. Spatiotemporal control of gene expression by a light-switchable transgene system. *Nature methods* **9**, 266-269, doi:10.1038/nmeth.1892 (2012).

20 Bugaj, L. J., Choksi, A. T., Mesuda, C. K., Kane, R. S. & Schaffer, D. V. Optogenetic protein clustering and signaling activation in mammalian cells. *Nature methods* **10**, 249-252, doi:10.1038/nmeth.2360 (2013).

21 Nihongaki, Y., Yamamoto, S., Kawano, F., Suzuki, H. & Sato, M. CRISPR-Cas9-based photoactivatable transcription system. *Chem Biol* **22**, 169-174, doi:10.1016/j.chembiol.2014.12.011 (2015).

22 Lee, S. *et al.* Reversible protein inactivation by optogenetic trapping in cells. *Nature methods* **11**, 633-636, doi:10.1038/nmeth.2940 (2014).

23 Dagliyan, O. *et al.* Engineering extrinsic disorder to control protein activity in living cells. *Science* **354**, 1441-1444, doi:10.1126/science.aah3404 (2016).

24 Gasser, C. *et al.* Engineering of a red-light-activated human cAMP/cGMP-specific phosphodiesterase. *Proc Natl Acad Sci U S A* **111**, 8803-8808, doi:10.1073/pnas.1321600111 (2014).

25 Wu, Y. I. *et al.* A genetically encoded photoactivatable Rac controls the motility of living cells. *Nature* **461**, 104-108, doi:10.1038/nature08241 (2009).

26 Strickland, D., Moffat, K. & Sosnick, T. R. Light-activated DNA binding in a designed allosteric protein. *Proc Natl Acad Sci U S A* **105**, 10709-10714, doi:10.1073/pnas.0709610105 (2008).

27 Lee, J. *et al.* Surface sites for engineering allosteric control in proteins. *Science* **322**, 438-442, doi:10.1126/science.1159052 (2008).

28 Polstein, L. R. & Gersbach, C. A. A light-inducible CRISPR-Cas9 system for control of endogenous gene activation. *Nat Chem Biol* **11**, 198-200, doi:10.1038/nchembio.1753 (2015).

29 Konermann, S. *et al.* Optical control of mammalian endogenous transcription and epigenetic states. *Nature* **500**, 472-476, doi:10.1038/nature12466 (2013).

30 Yazawa, M., Sadaghiani, A. M., Hsueh, B. & Dolmetsch, R. E. Induction of protein-protein interactions in live cells using light. *Nat Biotechnol* **27**, 941-945, doi:10.1038/nbt.1569 (2009).

31 Taslimi, A. *et al.* Optimized second-generation CRY2-CIB dimerizers and photoactivatable Cre recombinase. *Nat Chem Biol* **12**, 425-430, doi:10.1038/nchembio.2063 (2016).

32 Kawano, F., Okazaki, R., Yazawa, M. & Sato, M. A photoactivatable Cre-loxP recombination system for optogenetic genome engineering. *Nat Chem Biol* **12**, 1059-1064, doi:10.1038/nchembio.2205 (2016).

33 Loros, J. J. & Dunlap, J. C. Genetic and molecular analysis of circadian rhythms in Neurospora. *Annual review of physiology* **63**, 757-794, doi:10.1146/annurev.physiol.63.1.757 (2001).

34 Zoltowski, B. D. *et al.* Conformational switching in the fungal light sensor Vivid. *Science* **316**, 1054-1057, doi:10.1126/science.1137128 (2007).

35 Huang, S., Heikal, A. A. & Webb, W. W. Two-photon fluorescence spectroscopy and microscopy of NAD(P)H and flavoprotein. *Biophysical journal* **82**, 2811-2825, doi:10.1016/S0006-3495(02)75621-X (2002).

36 Froehlich, A. C., Noh, B., Vierstra, R. D., Loros, J. & Dunlap, J. C. Genetic and molecular analysis of phytochromes from the filamentous fungus Neurospora crassa. *Eukaryotic cell* **4**, 2140-2152, doi:10.1128/EC.4.12.2140-2152.2005 (2005).

37 Vaidya, A. T., Chen, C. H., Dunlap, J. C., Loros, J. J. & Crane, B. R. Structure of a light-activated LOV protein dimer that regulates transcription. *Sci Signal* **4**, ra50, doi:10.1126/scisignal.2001945 (2011).

38 Hirrlinger, J. *et al.* Split-cre complementation indicates coincident activity of different genes in vivo. *PloS one* **4**, e4286, doi:10.1371/journal.pone.0004286 (2009).

39 Jullien, N., Sampieri, F., Enjalbert, A. & Herman, J. P. Regulation of Cre recombinase by ligand-induced complementation of inactive fragments. *Nucleic Acids Res* **31**, e131 (2003).

40 Wang, P. *et al.* Intersectional Cre driver lines generated using split-intein mediated split-Cre reconstitution. *Scientific reports* **2**, 497, doi:10.1038/srep00497 (2012).

41 Guo, F., Gopaul, D. N. & van Duyne, G. D. Structure of Cre recombinase complexed with DNA in a site-specific recombination synapse. *Nature* **389**, 40-46, doi:10.1038/37925 (1997).

42 Cardin, J. A. *et al.* Driving fast-spiking cells induces gamma rhythm and controls sensory responses. *Nature* **459**, 663-667, doi:10.1038/nature08002 (2009).

43 Anastassiadis, K. *et al.* Dre recombinase, like Cre, is a highly efficient site-specific recombinase in E. coli, mammalian cells and mice. *Dis Model Mech* **2**, 508-515, doi:10.1242/dmm.003087 (2009).

44 Sauer, B. & McDermott, J. DNA recombination with a heterospecific Cre homolog identified from comparison of the pac-c1 regions of P1-related phages. *Nucleic Acids Res* **32**, 6086-6095, doi:10.1093/nar/gkh941 (2004).

45 Lo, C. A. *et al.* Quantification of Protein Levels in Single Living Cells. *Cell Rep* **13**, 2634-2644, doi:10.1016/j.celrep.2015.11.048 (2015).

46 Sando, R., 3rd *et al.* Inducible control of gene expression with destabilized Cre. *Nature methods* **10**, 1085-1088, doi:10.1038/nmeth.2640 (2013).

47 Andrews, B. J., Proteau, G. A., Beatty, L. G. & Sadowski, P. D. The FLP recombinase of the 2 micron circle DNA of yeast: interaction with its target sequences. *Cell* **40**, 795-803 (1985).

48 Chen, Y., Narendra, U., Iype, L. E., Cox, M. M. & Rice, P. A. Crystal structure of a Flp recombinase-Holliday junction complex: assembly of an active oligomer by helix swapping. *Mol Cell* **6**, 885-897 (2000).

49 Raymond, C. S. & Soriano, P. High-efficiency FLP and PhiC31 site-specific recombination in mammalian cells. *PloS one* **2**, e162, doi:10.1371/journal.pone.0000162 (2007).

50 Daigle, T. L. *et al.* A Suite of Transgenic Driver and Reporter Mouse Lines with Enhanced Brain-Cell-Type Targeting and Functionality. *Cell* **174**, 465-480 e422, doi:10.1016/j.cell.2018.06.035 (2018).

51 Madisen, L. *et al.* Transgenic mice for intersectional targeting of neural sensors and effectors with high specificity and performance. *Neuron* **85**, 942-958, doi:10.1016/j.neuron.2015.02.022 (2015).

52 Madisen, L. *et al.* A robust and high-throughput Cre reporting and characterization system for the whole mouse brain. *Nat Neurosci* **13**, 133-140, doi:10.1038/nn.2467 (2010).

53 Chan, K. Y. *et al.* Engineered AAVs for efficient noninvasive gene delivery to the central and peripheral nervous systems. *Nat Neurosci* **20**, 1172-1179, doi:10.1038/nn.4593 (2017).

54 Reed, W. A., Yan, M. F. & Schnitzer, M. J. Gradient-index fiber-optic microprobes for minimally invasive in vivo low-coherence interferometry. *Opt Lett* **27**, 1794-1796 (2002).

55 Gong, H. *et al.* High-throughput dual-colour precision imaging for brain-wide connectome with cytoarchitectonic landmarks at the cellular level. *Nat Commun* **7**, 12142, doi:10.1038/ncomms12142 (2016).

56 Schindler, S. E. *et al.* Photo-activatable Cre recombinase regulates gene expression in vivo. *Scientific reports* **5**, 13627, doi:10.1038/srep13627 (2015).

57 Boulina, M., Samarajeewa, H., Baker, J. D., Kim, M. D. & Chiba, A. Live imaging of multicolor-labeled cells in Drosophila. *Development* **140**, 1605-1613, doi:10.1242/dev.088930 (2013).

58 Hochbaum, D. R. *et al.* All-optical electrophysiology in mammalian neurons using engineered microbial rhodopsins. *Nature methods* **11**, 825-833, doi:10.1038/nmeth.3000 (2014).

59 Tsutsui, H., Karasawa, S., Okamura, Y. & Miyawaki, A. Improving membrane voltage measurements using FRET with new fluorescent proteins. *Nature methods* **5**, 683-685, doi:10.1038/nmeth.1235 (2008).

60 Chen, T. W. *et al.* Ultrasensitive fluorescent proteins for imaging neuronal activity. *Nature* **499**, 295-300, doi:10.1038/nature12354 (2013).

61 Pala, A. & Petersen, C. C. In vivo measurement of cell-type-specific synaptic connectivity and synaptic transmission in layer 2/3 mouse barrel cortex. *Neuron* **85**, 68-75, doi:10.1016/j.neuron.2014.11.025 (2015).

62 Joyner, A. L. & Zervas, M. Genetic inducible fate mapping in mouse: establishing genetic lineages and defining genetic neuroanatomy in the nervous system. *Dev Dyn* **235**, 2376-2385, doi:10.1002/dvdy.20884 (2006).

63 Dimidschstein, J. *et al.* A viral strategy for targeting and manipulating interneurons across vertebrate species. *Nat Neurosci* **19**, 1743-1749, doi:10.1038/nn.4430 (2016).

64 Liu, Y. J. *et al.* Tracing inputs to inhibitory or excitatory neurons of mouse and cat visual cortex with a targeted rabies virus. *Curr Biol* **23**, 1746-1755, doi:10.1016/j.cub.2013.07.033 (2013).

65 Tervo, D. G. *et al.* A Designer AAV Variant Permits Efficient Retrograde Access to Projection Neurons. *Neuron*, doi:10.1016/j.neuron.2016.09.021 (2016).

66 Cetin, A., Komai, S., Eliava, M., Seeburg, P. H. & Osten, P. Stereotaxic gene delivery in the rodent brain. *Nature Protocols* **1**, 3166-3173 (2006).

67 Franklin, K. B. J., & Paxinos, G. *The mouse brain in stereotaxic coordinates*. Vol. 18th Edition (1997).

68 Cho, J. R. *et al.* Dorsal Raphe Dopamine Neurons Modulate Arousal and Promote Wakefulness by Salient Stimuli. *Neuron* **94**, 1205-1219.e1208, doi:https://doi.org/10.1016/j.neuron.2017.05.020 (2017).

69 Gang, Y. *et al.* Embedding and Chemical Reactivation of Green Fluorescent Protein in the Whole Mouse Brain for Optical Micro-Imaging. *Front Neurosci* **11**, 121, doi:10.3389/fnins.2017.00121 (2017).

70 Li, A. *et al.* Micro-optical sectioning tomography to obtain a high-resolution atlas of the mouse brain. *Science* **330**, 1404-1408, doi:10.1126/science.1191776 (2010).